UNIVERSIDADE FEDERAL DE MINAS GERAIS
PROGRAMA DE PÓS-GRADUAÇÃO EM FÍSICA

Rafael Ricardo Rojas López

OPTICAL PROPERTIES OF TRANSITION METAL DICHALCOGENIDES ON GaAs

Belo Horizonte
2018

Rafael Ricardo Rojas López

OPTICAL PROPERTIES OF TRANSITION METAL DICHALCOGENIDES ON GaAs

Dissertation presented to the Graduate Program in Physics of the Instituto de Ciências Exatas of the Universidade Federal de Minas Gerais as a partial requirement to obtain the title of Master in Physics.

Supervisor: Paulo Sergio Soares Guimarães

Belo Horizonte

2018

Dados Internacionais de Catalogação na Publicação (CIP)

R628o Rojas López, Rafael Ricardo.
Optical properties of transition metal dichalcogenides on GaAs / Rafael Ricardo Rojas López. – 2018.
73f.

Orientador: Paulo Sérgio Soares Guimarães.
Dissertação (mestrado) – Universidade Federal de Minas Gerais – Departamento de Física.
Bibliografia: f. 59-69.

1. Propriedades ópticas. 2. Matéria condensada. 3. Espectros moleculares. I. Título. II. Guimarães, Paulo Sérgio Soares. III. Universidade Federal de Minas Gerais, Departamento de Física.

CDU – 535(043)

Ficha catalográfica elaborada por Gislene Rodrigues da Silva – CRB-6/3293
Biblioteca Professor Manoel Lopes de Siqueira – Departamento de Física - UFMG

Universidade Federal de Minas Gerais
Instituto de Ciências Exatas
Programa de Pós-Graduação em Física
Caixa Postal 702
30.123-970 Belo Horizonte - MG - Brasil

Telefone (xx) (31) 3499 5637
(xx) (31) 3499 5633
Fax (xx) (31) 3499 5688
(xx) (31) 3499 5600
e-mail pgfisica@fisica.ufmg.br

ATA DA SESSÃO DE ARGUIÇÃO DA 614ª DISSERTAÇÃO DO PROGRAMA DE PÓS-GRADUAÇÃO EM FÍSICA DEFENDIDA POR RAFAEL RICARDO ROJAS LÓPEZ, orientado pelo professor Paulo Sérgio Soares Guimarães para obtenção do grau de **MESTRE EM FÍSICA**. Às 09:00 horas de onze de setembro de 2018, na sala 4129 do Departamento de Física da UFMG, reuniu-se a Comissão Examinadora, composta pelos professores **Paulo Sérgio Soares Guimarães** (Orientador - Departamento de Física/UFMG), **Leonardo Cristiano Campos** (Departamento de Física/UFMG) e **Juliana Caldeira Brant** (Departamento de Física/UFMG) para dar cumprimento ao Artigo 37 do Regimento Geral da UFMG, submetendo o bacharel **RAFAEL RICARDO ROJAS LÓPEZ** à arguição de seu trabalho de dissertação, que recebeu o título de **"Optical properties of transition metal dichalcogenides on GaAs"**. Às 14:00 horas do mesmo dia o candidato fez uma exposição oral de seu trabalho durante aproximadamente 50 minutos. Após esta, os membros da comissão prosseguiram com a sua arguição e apresentaram seus pareceres individuais sobre o trabalho, concluindo pela aprovação do candidato.

Belo Horizonte, 11 de setembro de 2018.

Prof. Paulo Sérgio Soares Guimarães
Orientador do estudante
Departamento de Física/UFMG

Prof. Leonardo Cristiano Campos
Departamento de Física/UFMG

Dra. Juliana Caldeira Brant
Departamento de Física/UFMG

Candidato

A mis padres Rosaura y Ricaurte
y a mi hermana Yamile

Acknowledgements

One person is not just the result of himself but a contribution of many other ones. In these two years, there were many people who have supported me in different ways. First, I want to thank my family, my parents to whom I dedicate this goal, and my sister for their eternal love and support. To Christophe, my uncles, aunts, cousins and all my family that were always supporting and encouraging me to achieve my objectives.

In second place I want to thank all the people who contributed in a most direct way to the development of this work. To my advisor Paulo Sergio, who received me very warmly, and was always able to answer my questions. For his patience, advices and all the physics that he taught me. To Jose David, Ingrid and Barbara, from whom I learn all the details of the experimental physics life. To Juliana and Jessica for their help in our attempt to transfer the single layers. To Campô and Geovani, for their disposition in the spectral measurements. To Amanda and Diego from LCPNano Lab, for their help in the spectral measurements. To Katherine for the filters without which the low temperature measurements would not have been possible. To the Professors Patricia Lustoza de Sousa (PUC-Rio), Mauricio Pines (UFRJ) and Juan Carlos González (UFMG) for the substrates.

Also, I want to thank all the people with whom I shared good moments in these two years. To Sergio and Luisa, because they were my two main supports. I can not thank you enough for all you have done and care about me.

To Elvis, Milena and the little Vicky, for their generous friendship and receiving me as a family member. To Alix, Eduard and Gabriela because they are not just roommates but a family. To Ezequiel, Patricia, Julian, Victoria, Luis and all my hispanic friends for each beer, talk, party and all the smiles together. To Thiago, Henrique, Anna e Tulio for making the Lab day most kind. To Clovis, Bonnie, Ludmila, Rodrigo, Renan, Leonardo, Ronaldo, Adalberto and all the kind people of the physics department for the reception

into the DF. Finally but not least, to Ángela, Lorena, Andrés, Jose and Mauricio, my friends in Colombia who supported me despite the distance.

To the agencies CAPES, FAPEMIG and CNPq for the financial support.

Resumo

Os Dicalcogenetos de Metais de Transição (TMDs) são estruturas cristalinas da forma MX_2, onde M é um metal de transição, como Mo ou W, e X é um calcogênio, como S ou Se. Eles são estruturas compostas por multicamadas tipo X-M-X com ligações covalentes na camada e de Van der Waals nas interfaces entre camadas. Quando a espessura é reduzida até o limite de uma camada, pode-se observar uma transição de um semicondutor de gap indireto para um com gap direto em frequências do visível e infravermelho próximo. Assim, os TMDs são bons candidatos para a implementação de dispositivos optoeletrônicos ultrafinos. Por esse motivo, assim como pelo seu interesse no estudo de novos fenômenos físicos, eles tem sido amplamente pesquisados na ultima década. Já está estabelecido que as propriedades óticas dos TMDs são fortemente afetadas pelo substrato. Neste trabalho apresentaremos como as propriedades óticas de três TMDs diferentes, MoS_2, WS_2 e WSe_2, mudam depois deles serem colocadas em substratos de GaAs. Foram investigadas amostras sobre três tipos de substratos: GaAs dopado p, GaAs dopado n, e GaAs não dopado. As monocamadas foram obtidas pelo método de exfoliação mecânica e transferidas ao substrato. Como os índices de refração do GaAs e dos TMDs são muito próximos, tornando muito dificil a visualizção das monocamadas transferidas, estabelecemos um procedimento apropriado para a localização e manipulação dessas monocamadas. Apresentamos a análise espectral da luminescência em cada caso assim como os seus espectros Raman. Achamos que os substratos de GaAs produzem alterações na luminescência dos TMDs que podem ser entendidas com base no alinhamento de bandas dos TMDs com o GaAs. Concluimos que as heteroestruturas GaAs/TMDs tem um grande potencial para aplicações como fotodetetores e celulas solares.

Palavras chave: Dicalcogenetos de Metais de Transição, GaAs, MoS_2, WS_2, WSe_2, heteroestrutura, monocamada.

Abstract

Transition metal dichalcogenides (TMDs) are crystalline structures of the form MX_2, where M is a transition metal, like Mo or W, and X is a chalcogenide, as S or Se. They are multilayer structures, with X-M-X covalent bonds within a layer and Van der Waals bonds at the interlayer interfaces. As the thickness is reduced from several layers to a single monolayer, a transition is observed from a semiconductor with indirect band gap to a direct band gap in the visible or near infrared frequencies. Therefore, the TMDs are good candidates for the implementation of ultra-thin optoelectronical devices. For this reason, and also for their interest in the study of new physical phenomena, they have been extensively investigated over the last decade. It is already well established that the optical properties of monolayer TMDs are strongly affected by the substrate. In this work, we will present how the optical properties of three different TMDs, MoS2, WS2 and WSe2, are modified by placing them on GaAs substrates. We investigate samples on three types of substrates: p-doped GaAs, n-doped GaAs and undoped GaAs. The monolayers were obtained by mechanical exfoliation and transfered to the substrates. Since the refraction indexes of GaAs and the TMDs are similar, we had to establish a procedure to locate and deal with suitable monolayers. We present a spectral analysis of the luminescence emission for each case, as well as their Raman spectra. We find that the GaAs substrates produce significant changes in the luminescence of the TMDs, which can be understood with basis on the band alignment of the TMD with GaAs. We conclude that GaAs/TMDs heterojunctions have a great potential for applications as photodetectors and solar cells.

Key words: Transition metal dichalcogenides, GaAs, MoS_2, WS_2, WSe_2, 2D materials, monolayer, optical properties.

Contents

Contents **9**

1 INTRODUCTION **11**

1.1 Motivation **11**

1.2 Physical system **12**

2 TRANSITION METAL DICHALCOGENIDES **14**

2.1 Structure **14**

2.2 Electronic Properties **16**

2.3 Excitonic Properties **18**

2.4 Optical Properties **20**

2.5 Substrate effects **22**

2.5.1 Charge transference 22

2.5.2 Strain effects 23

2.5.3 GaAs properties 25

2.6 Monolayer Production **26**

2.6.1 Mechanical Exfoliation 26

2.6.2 Chemical Vapor Deposition 27

2.6.3 Physical Vapor Deposition 27

2.7 State of the art **28**

2.7.1 *Interface designed MoS2/GaAs heterostructure solar cell with sandwich stacked hexagonal boron nitride* [1] 28

2.7.2 *Monolayer MoS2/GaAs heterostructure self-driven photodetector with extremely high detectivity* [2] 29

2.7.3 *Large Lateral Photovoltaic Effect in MoS2/GaAs Heterojunction* [3] 30

2.7.4 *The effect of the substrate on the Raman and photoluminescence emission of single-layer MoS_2* [4] 31

3 EXPERIMENTAL SETUP **33**

3.1 Sample fabrication **33**

3.2 Raman Spectroscopy **35**

3.3 Photoluminescence Spectroscopy **37**

3.3.1 Low temperature Photoluminescence 38

4 RESULTS - TMDS ON GaAs **40**

4.1 Raman spectrum **41**

4.2 Photoluminescence 46

5 CONCLUSIONS AND PERSPECTIVES 57

BIBLIOGRAPHY 59

APPENDIX 70

A – DATA FILTERING 71

B – PL EXPERIMENTAL VALUES 72

CHAPTER 1

Introduction

The present work will be divided into five chapters. In chapter one, the reader can find a brief introduction to the topic. Here we will explain the interest of our work as well as its main idea. The second chapter will present the whole necessary theory to understand the main features of the TMDs and what is the state of the art, of our topic, through a summary of the more relevant works in literature. In chapter three we will show and explain the experimental techniques used for the analysis of the samples. Chapter four contains all the spectral results and their analysis through a band offset proposition and finally, in chapter five we will present the conclusions and perspectives of the entire work.

1.1 Motivation

Development of new and better electronic devices imply in the improvement of their internal components. In 2004 Novoselov *et al.* found a bidimensional crystal of carbon atoms: graphene [5]. This new material consisting of a monoatomic carbon layer exhibits several interesting properties such as flexibility, better electrical conductivity than metals, very high tensile strength, among others. It can be classified as a semiconductor but with a zero band gap. Graphene research is still raising in a dramatical way pointing it to be the solution for several technological challenges.

Graphene lack of a band gap gives rise to interesting properties but is also a disadvantage for some applications. There are some ways to produce a gap in graphene [6] but for an application that requires a low dimensional semiconductor there are many other 2D materials that can be considered, like black phosphorus (BP), hexagonal boron nitride

(hBN) and transition metal dichalcogenides (TMDs).

Transition metal dichalcogenides are a family of materials with the form MX_2, with M a transition metal and X a chalcogenide. They are multilayer structures, with X-M-X covalent bonds within a layer and van der Waals bonds at the interlayer interface. This graphene-like configuration allows the fabrication of monolayer samples through techniques like mechanical exfoliation or chemical vapor deposition (CVD).

It was found that at the monolayer limit the TMD presents a transition from a semiconductor with an indirect gap to a semiconductor with a direct gap, enabling a more efficient electronic transition [7] [8] [9]. This transition to a direct gap increases remarkably the intensity of light emission, producing photoluminescence in the visible and near-infrared region.

These properties have attracted great interest because of their huge potential for the development of more efficient devices for optoelectronic applications (phototransistors [10], photodetectors [11], sensors [12], solar cells [13], etc) and basic research (single photon generation [14], etc) as well as their already established use at the industry as a dry lubricant [15].

1.2 Physical system

As already mentioned, the TMDs have interesting properties for technological development, in that way, there are many variables that can enhance or produce worse devices. We will study in this work the effect of some of those variables. One of them is the substrate; due to the strong electronic interaction with the TMD monolayer, the substrate affects the optical properties of the semiconductor in a significant way [16] [17] [18] [19].

First of all, it is important to study the best way to obtain larger TMD monolayers on the substrate for the future realization of devices, including electrical contacts fabrication. In this work, we will use the mechanical exfoliation method by direct transference to the substrate and by gel film transference. The most efficient method of exfoliation will be determined, taking into account effects like size, contrast, time of production among others. Roughness in monolayers is also an important factor to take into account because it can cause interference effects at different points of the sample in addition to the different interaction with the substrate at each point [16].

It is well known that GaAs has a high electron mobility and a direct band gap, which makes it a good candidate to be used in technological devices [2]. So, to study the influence of the substrate and the suitable properties of GaAs, we will study the optical properties of different TMDs over three kinds of GaAs: p-doped, n-doped and undoped, looking for the ideal one for future applications and determining the differences in theire

behavior. Differences are to be expected since it has already been shown that charge transfer occurs between the TMDs and the substrate. The different band alignments and charge concentrations of the different substrates should lead to differences in the optical emission.

Changes in the optical properties have been reported due to temperature dependence: improvement of photoresponse by interface effects reduction [20], new photoluminescence peaks emerging [21] [22] , changes of intensity between mono and bilayer cases [23], etc. In this way, we will study possible changes in the optical properties of our system TMD/GaAs at low temperature.

We studied the three more popular TMDs: MoS_2, WS_2 and WSe_2 owing to their differences in the band structure (and consequently in its emission energy) which can lead to a better response of one of them for possible future applications.

CHAPTER 2

Transition Metal Dichalcogenides

Transition Metal Dichalcogenides (TMDs), as aforementioned, are a family of materials with the general formula MX_2 with M a Transition Metal and X a Chalcogenide. There are around sixty different TMDs which can vary from insulators to metals and around two-thirds of them are layered materials [24]. These last ones can also have different properties depending on the physical and electronic features of the transition metal and the chalcogenide. In that way, we will present below the principal properties but focus on the three TMDs studied on this work.

2.1 Structure

Different from graphene, TMDs are not mono-atomic layer structures, instead they present a sandwich-like configuration with the transition metal in the middle of two chalcogenide layers (see Figure 1). Depending on the constituent atoms of the TMD, it can be arranged in two principal configurations (phases) trigonal prismatic $(2H)$[1] or octahedral $(1T)$ [25] (Figure 1). The prismatic phase is the one normally found in thermal equilibrium at room temperature [26], however the 1T phase can often be obtained as a metastable one [27]. Also, there are several polytypes due to the displacement of some of the atoms with respect to the lattice *e.g.* a transition metal displacement from the dichalcogenides [24]. However, for our work: WS_2, WSe_2 and MoS_2, have all a prismatic

[1] In this convention, H represents the hexagonal character of the lattice and 2, the number of layers in the unit cell. Properly speaking, in the monolayer limit there is not necessarily the number 2, however, convention is maintained.

configuration under mechanical exfoliation condition [2].

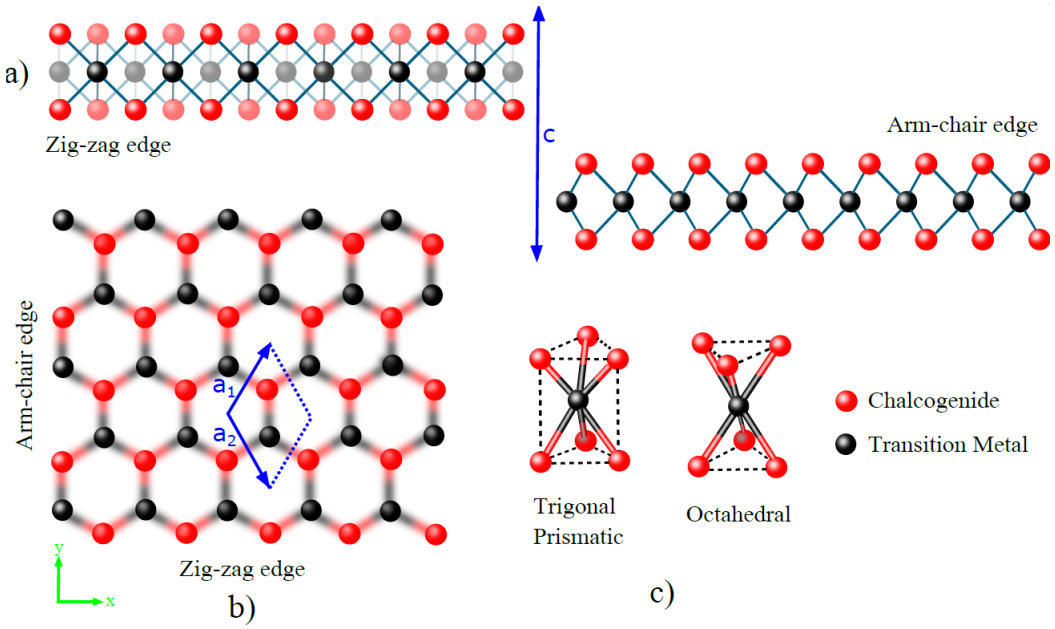

Figure 1 – a) Side view of typical TMD layers XZ plane (left) and YZ plane (right). b) Top view of the lattice and c) the two principal phases of layered TMDs.

In its $2H$ phase, TMDs have a top view of a honeycomb lattice just like graphene, in this way, we will define the primitive vectors a_1 and a_2 at the layer plane equal to their graphene analogous, and the third vector, c, will describe the interlayer periodicity (Figure 1) which, due to thermal equilibrium condition, is of two layers (Figure 2.a). Table 1 presents the lattice parameters for the three TMDs.

TMD	a (Å)	c (Å)
MoS_2	3.162	12.29
WSe_2	3.286	12.99
WS_2	3.162	12.37

Table 1 – Experimental lattice parameters [29].

It is possible to express the two lattice vectors, in the atomic layer plane, in therms of the inter-atomic distance a, as $a_1 = \frac{a}{2}(1, \sqrt{3})$ and $a_2 = \frac{a}{2}(1, -\sqrt{3})$. With these vectors it is possible to find their analogous in the reciprocal space $b_1 = \frac{2\pi}{a}(1, \frac{1}{\sqrt{3}})$ and $b_2 = \frac{2\pi}{a}(1, -\frac{1}{\sqrt{3}})$ which describe the reciprocal lattice that is also a hexagonal one. The Brillouin zone in the reciprocal space shows the high symmetry points (Figure 2.b) , which are important for electric band modeling, as it will be explained bellow.

[2] The $1T$-phase can be reached through lithium exfoliation [28].

2.2 Electronic Properties

The determination of the wave function of all electrons in a crystalline structure, like that of the TMDs, is not a straightforward work if an exact solution of the Schrödinger equation is tried. When all interactions are considered, one has a set of 3N coupled second order differential equations. Even numerical solutions become an impossible task, because of the number of electrons in a crystal (N) tends to the thermodynamic limit. In this way, approximations have to be used, like the Hartree-Fock method. Nevertheless, in 1998 Walter Kohn and John Pople found a new way to resolve this problem, with the development of the Density Functional Theory (DFT) [30]. On their work, they did not use individual properties of atoms or wave functions but their collective properties like the electron density.

However, different analytic approaches were also developed to study these systems, as the **k·p** theory [31] or the tight binding model [32]. In both cases symmetry considerations are taken into account, although in the first one, a perturbative study is developed while in the second one a superposition of individual electronic states of atoms is made, *e.g.* at the TMDs: chalcogenides provides the dominant *p-orbitals* while transition metals, the *d-orbitals* [33] [34].

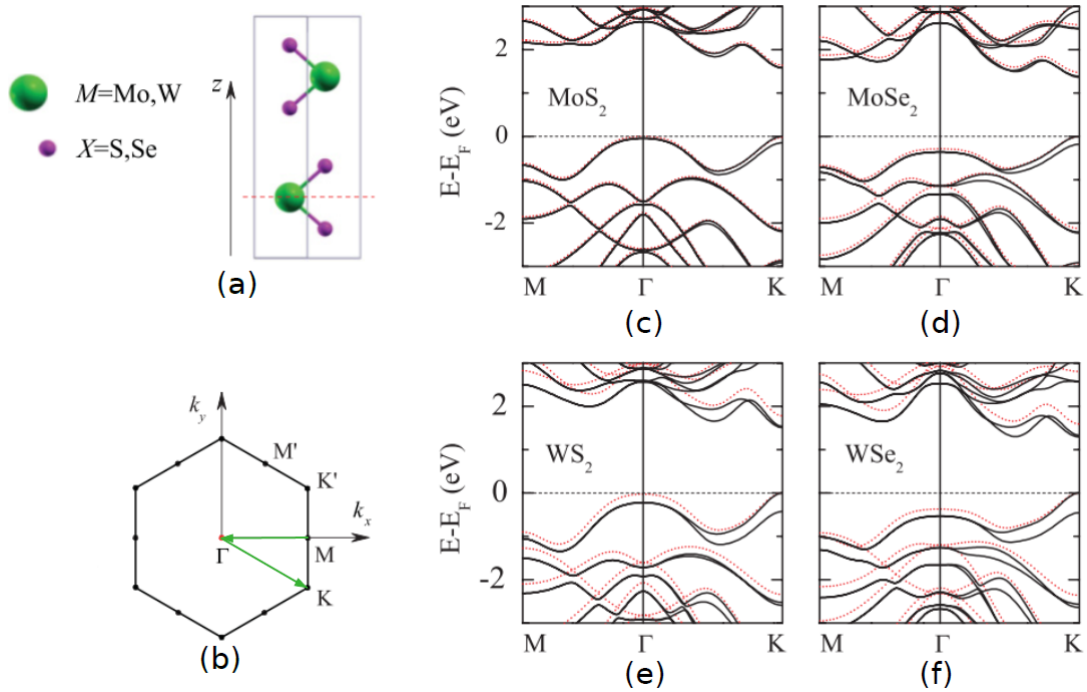

Figure 2 – (a) Profile view of a bilayer section from a TMD. (b) First Brillouin zone with the high symmetry points. (c)-(f) Electronic band structures for the principal TMD monolayer: with (solid line) and without (dotted line) inclusion of the spin-orbit interaction. Figure modified from [35].

The analysis of the electronic properties is made using the reciprocal lattice generated by all wave vectors **k** that yield plane waves with the periodicity of the crystal lattice [36]. On the space generated by these vectors (reciprocal space), it is possible to construct a unit cell with the smallest area possible, which is called the first Brillouin zone. Because this cell is able to reproduce all the lattice, the study of the states on it, is enough to describe all the crystal. On figure 2.b it is presented the Brillouin zone of a TMD monolayer and its high symmetry points, and also, (in green) the path along which the band structure shown in Figures 2 c-f is calculated.

When individual electronic states of all the crystal are represented on the space, bands of states will appear. Depending on how is the relation between these bands and the Fermi level it is possible to classify the material as a metal, if the Fermi level is on the middle of a band, semiconductor, if it is placed on the middle of two bands with a separation less than $\approx 3\ eV$, or insulating if this separation is larger. In this way, the bands above and bellow the Fermi level are called conduction and valence band, respectively. The separation between the conduction and the valence bands is called the "band gap". Table 2 presents the band gaps of the TMDs of interest to this work.

Concerning the exchange of energy with photons, three different electronic processes can occur on the crystal: first, absorption process, in which an electron passes to a higher energy level by a photon absorption. Second, photon emission by spontaneously decay of the electron to a lower energy level and finally, a transition to a less energetic level by being stimulated externally by a photon [37]. The minimum energy for the photons in all these processes occurs when the electronic levels involved are the valence band maximum (VBM) and the conduction band minimum (CBM).

Nevertheless, VBM and CBM do not necessarily occur at the same point in k-space. It is possible to classify a semiconductor by the alignment of the valence and conduction band extrema in direct or indirect band gap semiconductors. In the first one, the VBM and CBM occurs at the same value of k-vector and the transition is purely photonic, while in the second case they are at different values of k and a phononic process is needed to allow the transition. TMDs in their bulk state are indirect band gap materials.

Symmetry considerations are also necessary to understand how electronic transitions and band structures are given on a crystal. In Figure 2(a) a profile view of a bilayer section of a TMD is presented. It is possible to see how in the monolayer limit an inversion symmetry breaking (ISB) takes place; it means: taking a Mo atom as a center of inversion, an S atom will be mapped onto an empty point [38] .

Also, MoS2 has a strong spin-orbit coupling (SOC) originated from the d orbitals of the heavy metal atoms. Thus, when SOC and ISB are taken into account, a spin-orbit splitting (SOS) will emerge and the band structure will change with particular importance at Γ and K points of the Brillouin zone (see Figure 2 (c)-(f)), but also in the inequivalent

K' points, with an inverse spin relation [39].

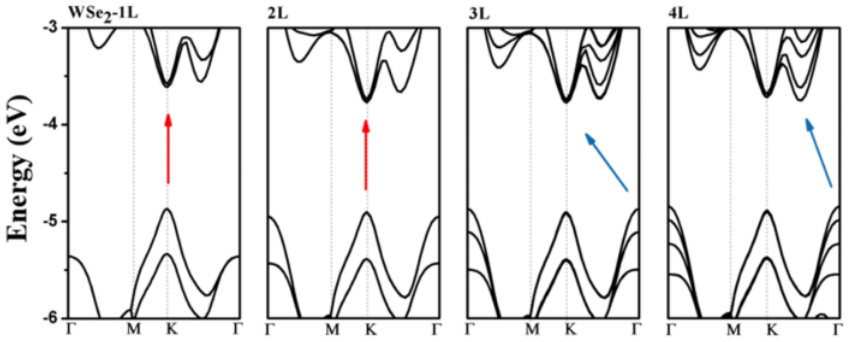

Figure 3 – Band structure evolution of WSe_2 as a function of the layer thickness. Figure taken from [35].

Further, achieving the monolayer limit induces an electron confinement in the z direction, producing an energy splitting at the Γ point due to the reduction of Van der Waals interactions. Due to this and the SOS, a transition to direct band gap (see Figure 3) takes place when the thickness is reduced to one (or two) monolayers.

2.3 Excitonic Properties

The excitons are bound states (also called quasiparticles) of an excited electron on the conduction band and a hole in the valence band through a Coulomb interaction. Therefore, there is a dependence of the exciton binding energy with the band structure but also with the dielectric constant. In that way, it is possible to classify the excitons in two types: Frenkel or Wannier-Mott. The first ones are present principally on organic crystals and have a large binding energy ($0.1\ eV - 1.0\ eV$). The second ones are usually present on semiconducting materials that have a large dielectric constant and, for this reason, binding energies are typically of the order of $0.01eV$, with exciton radius larger than Frenkel ones [26].

Exciton binding energy depends also on the dimensionality, it means, excitons on two-dimensional materials will have larger binding energies than in their bulk counterparts. On this way, excitons in 2D TMDs will usually exhibit a Frenkel character. Nevertheless, large exciton radius has been also reported for TMDs giving to them a Wannier-Mott character.

Other bound states, besides the exciton, can be found in nature; it is the case of the trion, also called positively (negatively) charged exciton, that consists of one exciton bound to a hole (electron). In addition, when exciton concentration is increased, two

excitons can be bound to form a biexciton. In Figure 4 a schematic view of the bound states in the K point of the Brillouin zone is presented .

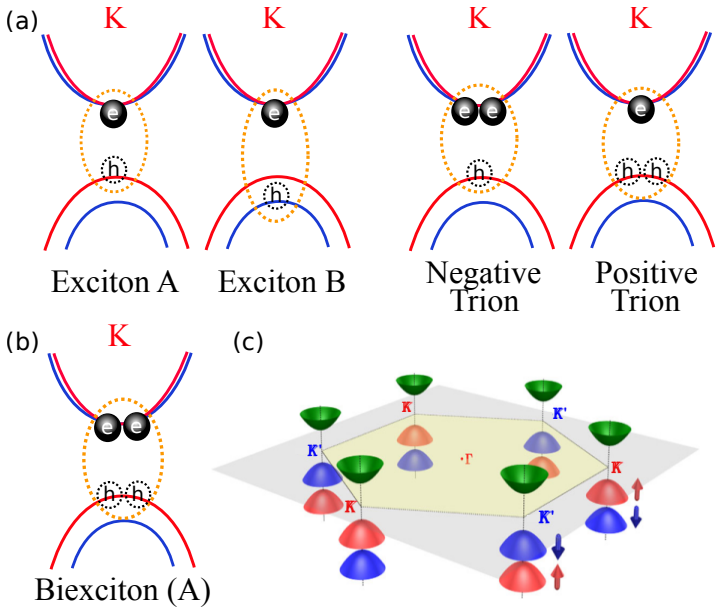

Figure 4 – (a)-(b) Representation of different bound states at the K point. (c) Schematic drawing of the band structure at the K and K' points representing the spin-up (red) and spin-down (blue) states. Modified from [38].

Despite the differences in the reported values, the binding energies of the TMD excitons are large as compared to the values of excitons in conventional semiconductors (Table 2). The excitons in TMDs have a lifetime of the order of few *ps* and can decay in a radiative way or by several pathways such as electron-phonon relaxation, Auger recombination [40], etc.

	MoS_2	WSe_2	WS_2
Band gap (eV)	1.90 [7]	1.72 [41]	2.11 [41]
Exciton BE (meV)	570 [42]	370 [43]	312 [44]
Trion BE (meV)	18 [45]	30 [46]	26 [47]
Biexciton BE (meV)	70 [48]	52 [49]	65 [50]

Table 2 – Experimental values of gap and binding energies (BE) in bound states at TMDs.

One of the effects of the SOS is the emergence of spin states that will produce two types of excitons in the K and K' points (see Figure 4) with opposite spin states. The binding of an electron on the CBM and a hole in the VBM will produce the A-exciton. On the other hand, an electron in the CBM can be bound with a hole at a less energetic spin state at the same point producing the so-called B-exciton. Due to the fact that they are located on local minima, the study of the interactions and control of the excitons in

these points is called valleytronics and, particularly, TMDs has been exhibit interesting properties for possible applications in this area [48].

2.4 Optical Properties

Interaction of light with matter can be classified into three types: reflection, propagation, and transmission. Furthermore, reflection can be seen as a specific case of scattering, a process in which light changes its trajectory and possibly its frequency, due to the changes in the medium. On the other hand, in the propagation process, light which enters the crystal can be absorbed when the frequency of incoming light is resonant with the transition frequencies of the atoms in the crystal. The excited atoms can decay to a low energy state, by a photon emission in a process called luminescence. The light will be emitted in all directions with a different frequency from the incoming beam[3]. Finally, light which is transmitted will be refracted in the process: the propagation velocity will change due to a propagation medium change [51].

Characterization of a material in each step above mentioned enables to know its classification and possible applications. In this work, we will focus on the luminescence process of TMDs which are closely related to the electronic structure and excitonic features explained before.

When the photons are absorbed by the TMDs, electrons will be promoted to the conduction band and excitons can appear. After electron energy relaxation, a photon with a different frequency from the incoming beam will be emitted, but also with an energy different from the electronic band gap of the material. This is due to the binding energy of the exciton. Therefore, the emission spectrum will have peaks on the exciton recombination energies, also called as the optical gap. In the same way, emissions from other quasiparticles like trions or biexcitons will also be detected. The whole set of emissions by recombination is known as photoluminescence (PL) spectrum, one kind of luminescence in which the material emits light due to optical excitation. Figure 5 (b)-(e) presents the characteristic photoluminescence spectrum of the TMDs monolayer.

A clear dominant A-exciton peak is seen in all different spectra, at 1.61 eV (765 nm) for WSe_2, 1.96 eV (633 nm) for WS_2 and 1.83 eV (678 nm) for MoS_2. Less intense B-exciton peak is presented in gray; it is many times weaker due to the much smaller transition probability from the electron in the conduction band to a lower valence band state. Although, depending on the monolayer production method, defects, temperature, etc. the B-exciton intensity would increase. Thus, small differences will emerge in the PL spectra in the literature [9] [45] [49]. Specifically, MoS_2 presents a partial overlapping of

[3] Although excited atoms does not always decay in a radiatively way. Energy can be dissipated, for instance by phonon emission.

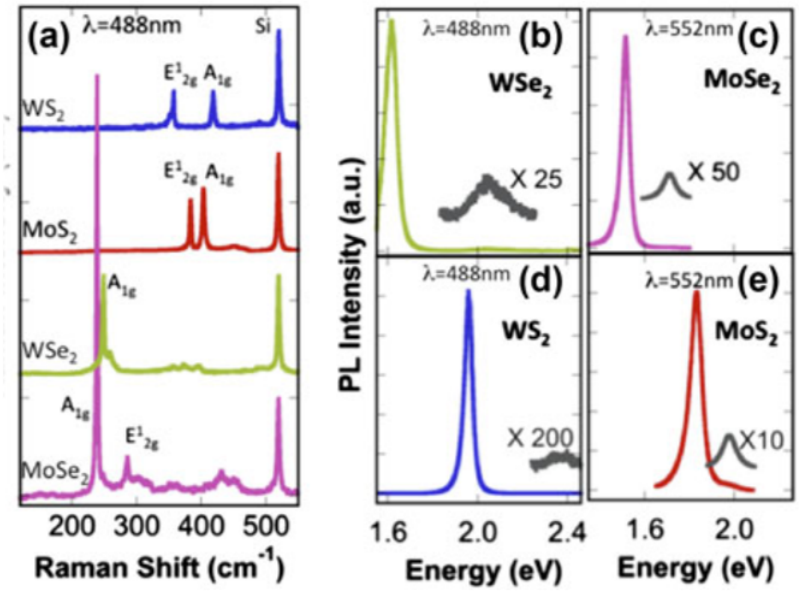

Figure 5 – Raman (a) and Photoluminescence (b)-(e) spectra of the TMDs monolayer on SiO_2. Taken from [52]

the two excitons due to the small SOS of the states making the transition more probable and intense. B-exciton energies are 2.04 eV (608 nm) for WSe_2, 2.34 eV (530 nm) for WS_2 and 1.98 eV (626 nm) for MoS_2.

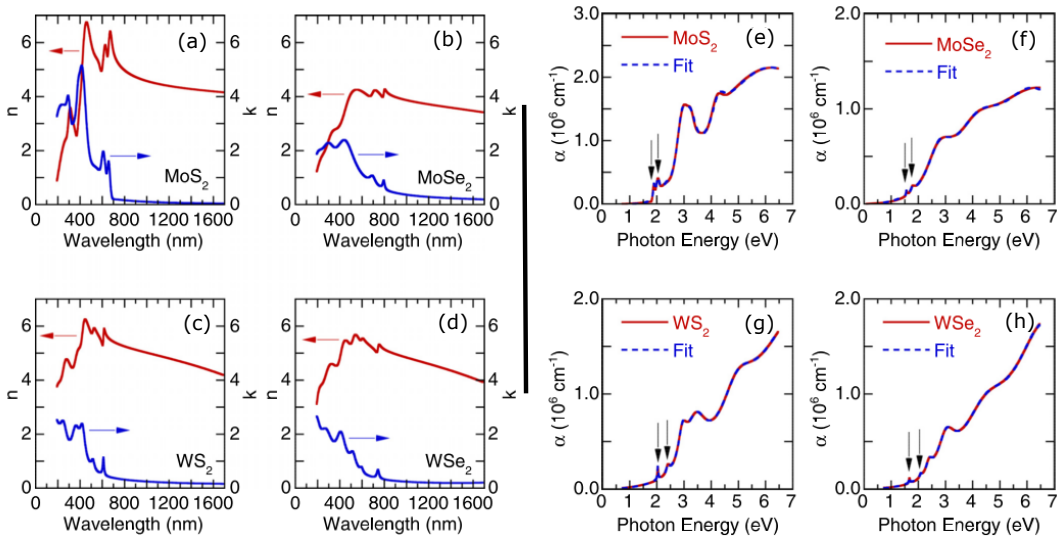

Figure 6 – Refractive index and extinction coefficient of (a)MoS_2 (b) $MoSe_2$ (c)WS_2 and (d)WSe_2. Absorption coefficient of (e)MoS_2 (f) $MoSe_2$ (g)WS_2 and (h)WSe_2. [41]

The complex refractive index $\bar{n} = n + i\kappa$ provides knowledge about the change in the beam velocity in the crystal (n) but also information about the system such as the extinction coefficient (κ), the absorption coefficient $\alpha = \frac{4\pi\kappa}{\lambda}$, as well as the dielectric

function of the crystal $n = \sqrt{\epsilon}$ [51]. Differences on the refractive index between the TMD and substrate, for instance, will be related to the optical contrast, providing information about the more efficient way for the monolayer identification. In Figure 6 (a)-(d), the refractive index n (red) and extinction coefficient (blue) of the main TMDs are presented. Additionally, Figures 6 (e)-(f) show the absorption coefficient indicating with arrows the position of the A and B-excitons. It is possible to see how photons with less energy than excitons are not absorbed by the TMDs; it is because the minimum of energy which produces a transition from valence to the conduction bands is, in fact, the exciton energy. Higher energy photons will be absorbed in many different pathways producing transitions between different bands.

2.5 Substrate effects

The properties of the TMDs can be affected in many different ways by roughness, defects in the crystal, temperature, etc. The substrate, for example, is in direct contact with the TMD playing a pivotal role in its properties. For instance, charge transfer between the substrate and the TMDs induces changes in the electronic and optical properties of the TMDs. Here we will focus principally on two types of substrate effects which affect the TMDs: strain and charge transference. Below, we will present a brief review of them but a full review of all substrate effects can be read at [16].

2.5.1 Charge transference

When a TMD is put on a substrate, electrons will be transferred to the material with smaller Fermi energy level. Thus, to understand how the charge transfer is performed, it is necessary to understand how the electronic band structure is at the junction. In MoS_2 on SiO_2, for instance, there is a rise on its Fermi level due to more electrons being transferred to the conduction band coming from the substrate and increasing the probability of formation of negatively charged excitons on the TMDs [53].

After the charge transference from the substrate to the TMD, exceeding electrons can link up to the excitons in the TMDs to form negatively charged excitons (negative trions). The PL spectrum thereby will show an increase on the respective trion peak and a corresponding decrease of the intensity of the uncharged exciton peak [4] [54].

Charge transference also occurs on a substrate such as Si/SiO_2, one of the most common in the literature. Silica substrate is a semiconductor material negatively charged which also will transfer charge to the TMD improving the trion emission. In Figure 7 the MoS_2 PL spectrum is presented, showing the position of the neutral excitons A^0 and B as well as the trion A^- on different substrates. A clear lower intensity for the PL spectra of

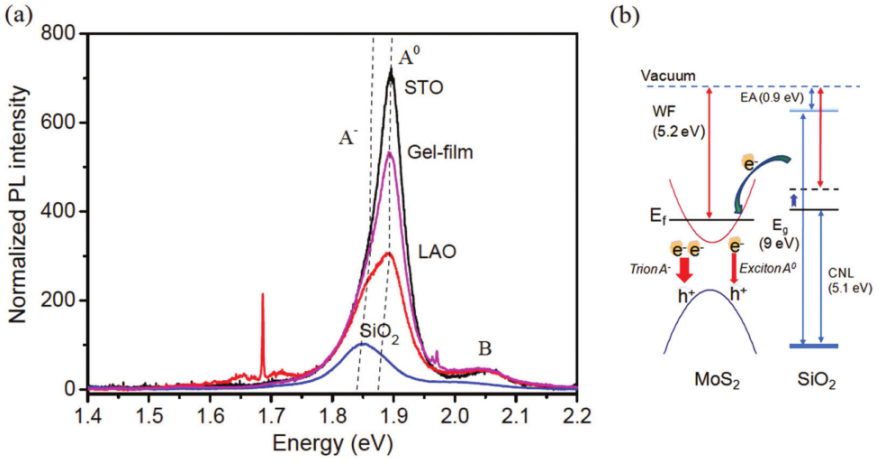

Figure 7 – (a) Photoluminescence of MoS_2 on different substrates $SrTiO_3$ (STO), Gel-film, $LaAlO_3$ (LAO) and SiO_2. (b) Schematic band structure alignment on the junction MoS_2/SiO_2 with the representation of the WF (work function), EA (the electron affinity) and CNL (charge neutrality level). Modified from [53]

MoS_2 on SiO_2 is visible, and also a dominance of the trion emission. A schematic band representation of the junction is proposed by the authors in 7.(b) [55].

In the exfoliation process, defects such as sulfur vacancies or water moisture can appear on the interface. They will induce a doping effect which improves the trion emission but increases the non radiatively exciton decay [56] [57]. Nevertheless, doping can improve general properties if it is correctly selected. Thus, the natural charge of the TMDs could give information about how the substrate should be. *Yu et al.* [56] propose that doping mitigation can be done through the use of p-doping substrates for the negatively charged WS_2 and MoS_2 while an n-doping substrate is suggested for the positively charged WSe_2.

2.5.2 Strain effects

Flexibility is one of the interesting properties of TMDs because of its potential applications in flexible devices [58] [59]. However, tensile strain affects the natural properties of the TMDs. When mechanically exfoliated monolayers are transferred to the substrate, roughness can appear and local variances on the mechanical and electrical properties can be produced [60].

Holes on the substrate can appear as undesirable defects or in a controlled way. A TMD monolayer transferred to a matrix of holes in the substrate has been studied in order to characterize its properties [61]. A PL enhancement was observed in the suspended single layer at each hole (Figure 8.b). The Raman spectrum is also modified on MoS_2. A displacement is produced on the in-plane E^1_{2g} Raman mode while the out-of-plane A_{1g} remains at its position [61] [55].

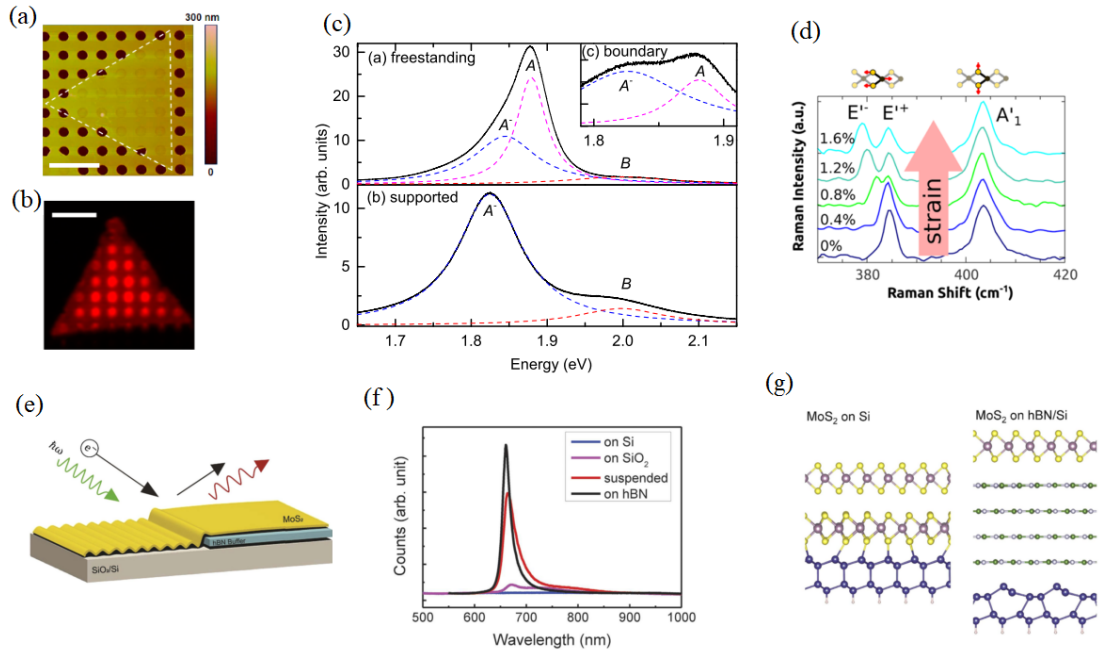

Figure 8 – (a) Atomic force microscopy (AFM) on a MoS_2 monolayer and its (b) Photoluminescence map. Scale bar 5 μm [61]. (c) MoS_2 PL spectrum in the freestanding and supported single layer [55]. (d) MoS_2 Raman spectrum under different applied strain [62] (e) Illustrative representation of a single layer over a thin hBN buffer on Silica substrate. (f) MoS_2 PL spectrum over different substrates and (g) representation of the interface bounding and distortions [63].

Moreover, strain can be produced by defects on the substrate or by a distorted crystalline structure of TMD with regard to the substrate. For example, strain can be produced by the non-symmetrical binding between the MoS_2 and Si/SiO_2 through the interface; it could produce a reduction of the photon emissions and thus a less intense PL and Raman spectrum. To prevent it, an isolation of MoS_2 is proposed though another layered material, hexagonal boron nitride (hBN). This arrangement leads to an enhancement of the TMD properties by decreasing the charge transfer, interface effects or roughness (Figure 8 (e)-(g)) [63].

Furthermore, the strain has also been studied by applying different quantities of it on a MoS_2 monolayer. As studied for charge transfer, a redshift on the PL spectrum occurs and a dramatical decrease of the intensity is detected. In the other hand, for strain up to 0.8%, the Raman E^1_{2g} in-plane mode will also present a redshift with a strain dependent peak splitting, while the A_{1g} mode remains unaffected (Figure 8) [62].

2.5.3 GaAs properties

Galium Arsenide is a crystalline material with a zinc blende lattice configuration[4] and a unit cube length of 5.65 Å. It is a semiconductor material with a direct band gap of 1.42 eV at room temperature [64]. It can be doped by replacing some gallium atoms in the lattice by, in our case, zinc atoms for a positive doping or by silicon atoms for negative doping.

Its Raman spectra will present a prominent longitudinal optical (LO) peak at 292 cm^{-1} and a small transverse optical (TO) peak in 267 cm^{-1} [65] for the undoped case (see Figure 9) whereas doped samples present a highly relevant TO peak which will vary depending on the doping level of the crystal [66]. Doped samples have an electron mobility of a few thousands $cm^2V^{-1}s^{-1}$ for a concentration of carriers of the order of 10^{18} cm^{-3} [67, 68].

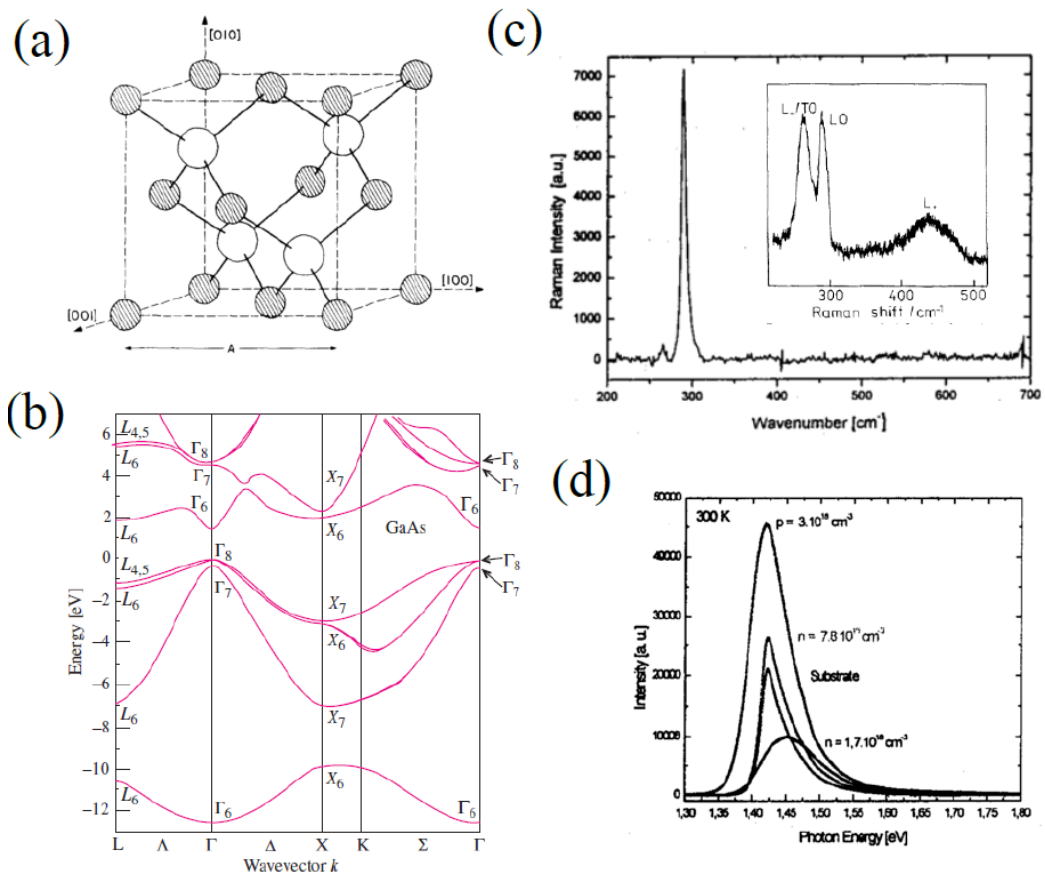

Figure 9 – Features of GaAs (a) Unitary cube structure [68], (b) band structure [69], (c) Raman spectrum of undoped and n-doped (inset) cases [70] [65] and its (d) PL for the p and n doped cases. [65].

Photoluminescence spectra will exhibit different features depending on the doping

[4] This is, in principle the face centered cubic (FCC) structures of an atomic species interpenetrated by a second FCC lattice of a different atomic species [36].

and temperature, usually presenting many peaks. Nevertheless a broad main peak at 1.42 eV at room temperature will be an important feature in particular for the doped cases.

2.6 Monolayer Production

Monolayers of transition metal dichalcogenides can be achieved in many ways. However, here we present the three most used methods in literature.

2.6.1 Mechanical Exfoliation

Owing to the TMD layered condition, disengagement of the layers can be made through the same graphene mechanical exfoliation[5] method: a piece of adhesive tape is placed over one seed[6] of the TMD and slowly peeled back off. Interlayer bonding within the films can be broken and small regions with material will be glued to the tape. Nevertheless, few or single layer regions will be less probable. Thereby, to improve the number of few-layer regions, the tape should be glued into itself and peeled it back of to make a new exfoliation of the TMD. Subsequently, few-layer regions in the tape are transferred to the previously prepared substrate. In the transference process, a final exfoliation is produced between tape and substrate. Finally, the substrate with potential monolayer is mapped with an optic microscope to identify the single layers by optical contrast.

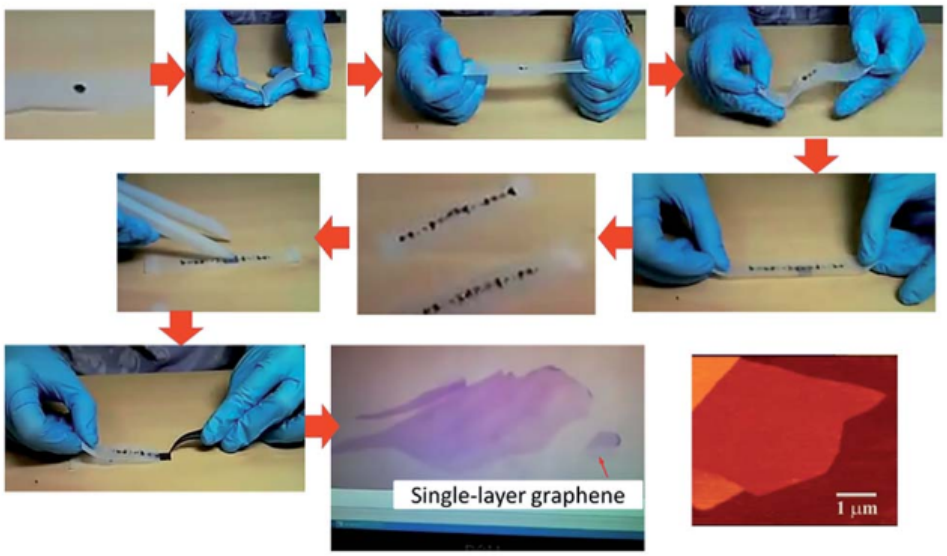

Figure 10 – Schematic illustration of mechanical exfoliation process. Taken from [71].

[5] Last folds extraction.
[6] A crystal seed is referred to be a small piece of the material used for sample fabrication.

2.6.2 Chemical Vapor Deposition

Chemical vapor deposition (CVD) is a method to produce thin films from precursors which react in vapor phase to generate a thin film on a given substrate. Different kinds of CVD procedures can be performed depending on the conditions in which they are made: pressure, precursors, temperature, etc. One of the methods used to grow TMD films is to place the substrate on a boat which will be put on a sapphire or quartz chamber, at vacuum, together with the MX_2 precursors. Subsequently, an initiator (H_2 for instance) gas is sent through the chamber and the vaporization process is made by heating them. TMD begins to link up over the surface of the substrate and depending on the time of interaction single or few layers can be formed on it.

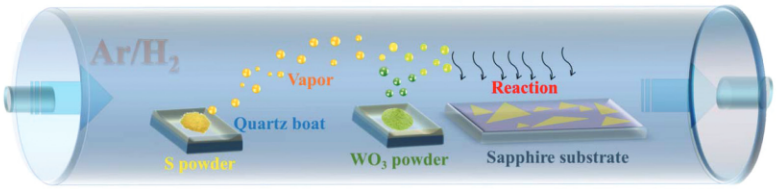

Figure 11 – Schematic illustration of the CVD set up. Taken from [72].

Another way to grow it is in two steps. A single film of the transition metal is grown on the substrate then CVD process is used to vaporize a dichalcogenide precursor to make it interact with the coated substrate. The difference with the first method is the achieving of large area monolayers due to the homogeneous film of transition metal precursor. However, it was found that CVD grow monolayer has less quality in comparison with other exfoliation methods. In [73] [74] is presented an extended review of the main methods, precursors and main features of the CVD grown single layers.

2.6.3 Physical Vapor Deposition

Physical Vapor Deposition (PVD) is closely related to the CVD process. While in CVD method precursors react in vapor phase to form the film, in PVD, precursors are in solid state. In PVD, substrate is put in a vacuum chamber along with the transition metal precursor target. Then, Argon gas is injected into the system. A magnetic field is applied to the target and Ar plasma is generated over it. Positively charged argon atoms will collide with the transition metal (TM) target and sputtering takes place. The TM atoms are adsorbed on the substrate and a thin film of TMD is produced. The result can, nevertheless, have impurities depending on factors like precursor target quality.

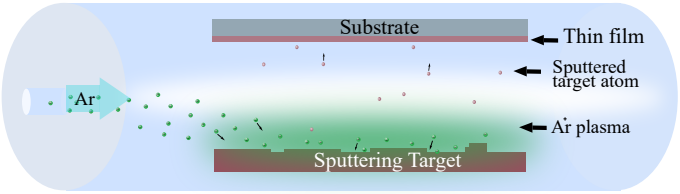

Figure 12 – Schematic illustration of the PVD set up.

2.7 State of the art

In the following, we will review the three more interesting studies that have been reported so far on TMDs on GaAs and also an investigation on the effect of different substrates on the optical properties of MoS_2.

2.7.1 *Interface designed MoS2/GaAs heterostructure solar cell with sandwich stacked hexagonal boron nitride* [1]

In this work, the authors made a solar cell with an n-type GaAs substrate and a MoS_2 monolayer. To make electrical measurements they used rear and frontal Au contacts, letting an open entrance region that allows light to interact with the MoS_2 monolayer (see Figure 13).

The MoS_2 monolayer is obtained through a chemical vapor deposition method (CVD) (see chapter 2.6.2) on a Si/SiO_2 substrate. After growth, they made a spun-on polymethilmethacrylate (PMMA) coating to paste the monolayer to it. This sample is immersed into deionized water to lift-off the PMMA-MoS_2 films. They are transferred to the n-GaAs and the PMMA coating is removed with acetone.

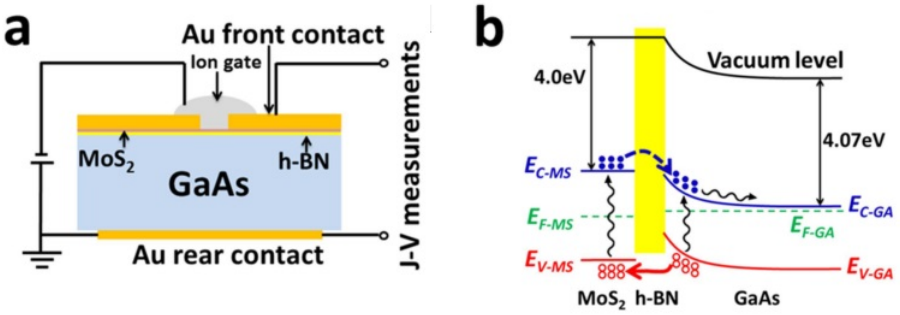

Figure 13 – a) Schematic structure and b) electronic band alignment of the MoS_2/hBN/GaAs solar cell. Taken from [1]

It is found that there is a static charge transfer from the n-GaAs substrate to the TMD monolayer, decreasing the solar cell efficiency. To eliminate the electron transference they put an h-BN monolayer in between the GaAs and MoS_2, which in fact let the substrate holes pass to the TMD, letting it positively charged and producing, in this way, the usual p-n junction of solar cells.

As a result, they obtain a power conversion efficiency (PCE) of 5.48% with the h-BN monolayer and 4.82% with the n-GaAs/MoS_2 original junction. To improve the solar cell PCE, MoS_2 is dopped with a nitromethane solution and an electrical gating is used too, obtaining a PCE of 9.03%, the highest value obtained for a TMD solar cell so far, in our knowledge.

2.7.2 *Monolayer MoS2/GaAs heterostructure self-driven photodetector with extremely high detectivity* [2]

In this work, the authors create a self-driven photodetector (zero external voltage) with a GaAs/h-BN/MoS_2/ Si QDs structure (see Figure 14). They use the same electronic band structure alignment from the last article for the n-GaAs/MoS_2 junction, as well as the use of h-BN to control the static charge transfer between the MoS_2 monolayer and the GaAs substrate.

In this device n-GaAs provides the majority charge carriers, the h-BN diminishes the dark current (detected current at static equilibrium) and finally, the QDs increase the absorption of light, especially for low power incident light, since the small thickness of the monolayer decreases its light absorption.

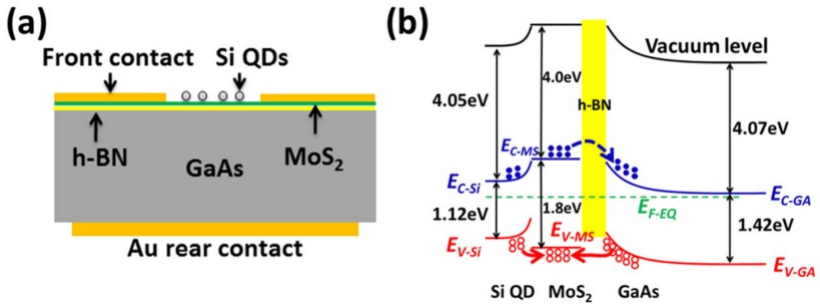

Figure 14 – a) Schematic structure and b) electronic band alignment of the QDs/MoS_2/hBN/GaAs photodetector. Taken from [2]

Finally, the photodetector is covered with a PMMA coating to conserve it. They obtain a responsivity of 419 mA/W and a detectivity of 1.9×10^{14} *Jones*.

2.7.3 *Large Lateral Photovoltaic Effect in MoS2/GaAs Heterojunction* [3]

The lateral photovoltaic effect (LPE) consists on the lateral flux of the photogenerated electrons and holes and their recombination on the same surface of the material, in other words, the flux of charges and the recombination occurs on the same side of the structure (see Figure 15 inset a). It's a useful property for the design of position sensitive detectors, since the lateral photovoltage measured between two contacts changes linearly with the position of the spot of illumination on the active region of the device.

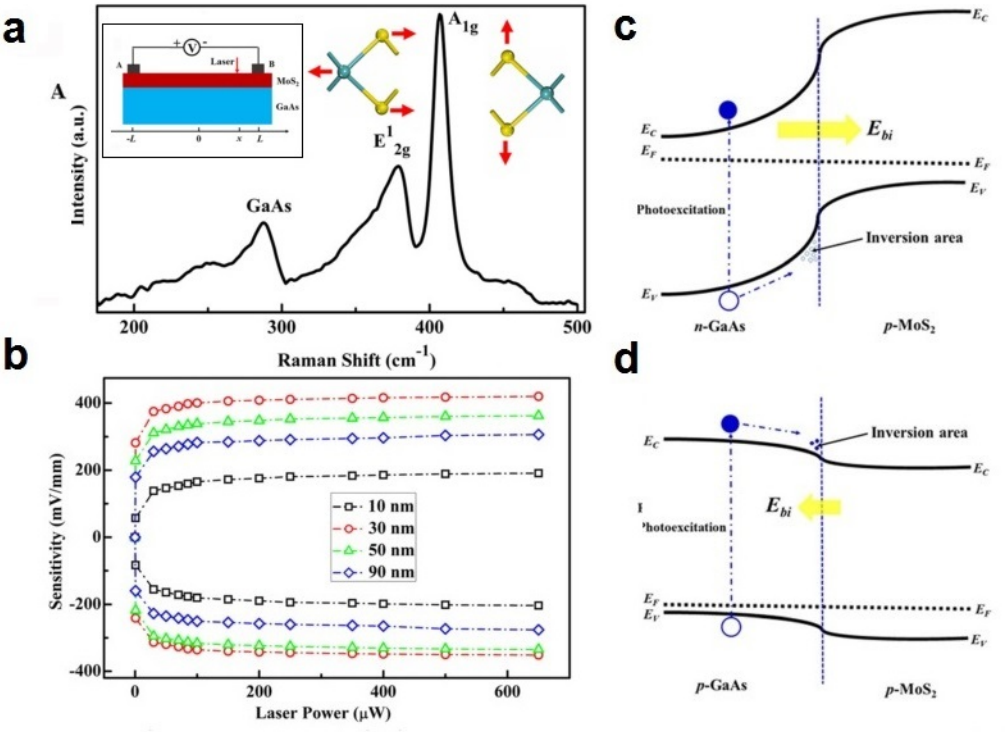

Figure 15 – a) Raman spectra of MoS_2 bulk with the two phonon modes. Inset: schematic structure of the device. b) Electric response of the device for different laser power and MoS_2 thickness. c) Electronic band alignment of the MoS_2/GaAs junction for p-type and d) n-type substrates. Taken from [3]

In this article, the authors study this effect on a MoS_2/GaAs junction. They work on n- and p-type GaAs substrates and different thicknesses of MoS_2 from 10 nm to 90 nm (see Figure 15 b). However, since the monolayer thickness is of $\approx 0.8\ nm$ [75], all this work is absolutely at the bulk limit.

To have a homogeneous thickness the authors grow the bulk through a physical vapor deposition method (see chapter 2.6.3) on GaAs. Through the voltage/current relations for each sample and a proposed band alignment for the junctions, they explain that there is a charge transference from the substrate to the MoS_2 bulk, of electrons for the n-type GaAs and of holes for the p-type one. They explain that due to that charge

transference a built-in field (E_{bi}) will appear in the interface producing an inversion layer.

They compare the results between n- and p-type substrates, finding that there is a much larger LPE for the n-type one, because of its electronic band alignment (see Figure 15 c and d) which lets the electrons be transferred to the TMD. Also, they conclude that the thickness with the best sensitivity is that one of 30 nm.

2.7.4 *The effect of the substrate on the Raman and photoluminescence emission of single-layer MoS_2* [4]

The authors studied dielectric substrates like SiO_2, Mica, Gel-Film and hexagonal boron nitride as well as conducting substrates such as Au and few-layer graphene (FLG). In this work, the authors consider effects such as the interference produced by the different interfaces and the charge transference between the materials.

To study the interference effect they take into account the multiple internal reflections at every interface media (Figure 16.a). They determine the light intensity absorbed and emitted by employing two methods, an effective medium approach and the transfer matrix formalism, getting consistent results. Using the intensity emission, they determine the enhancement factor

$$\Gamma^{-1} = \frac{I_{MoS_2}^{freestanding}}{I_{MoS_2}^{onsubstrate}}$$

where $I_{MoS_2}^{freestanding}$ is the emission intensity from the freestanding monolayer MoS_2 and $I_{MoS_2}^{onsubstrate}$ is the total emission intensity from the monolayer on a substrate. Thus, they plot the enhancement factor as a function of the wavelength for different substrates (Figure 16.b) producing changes on the spectral intensities.

After they measure the Raman and photoluminescence spectra, they normalize them by the enhancement factor (Figures 16.c and 16.e). Although, interference considerations do not change the spectral peak positions, differences are appreciated on both Raman and PL spectra.

For the Raman case, considerable changes are observed just in the A_{2g}^1 mode while differences of less than 0.4 cm^{-1} were observed in the E_{1g} mode (Figure 16.d). The authors also inform uniformity along the monolayer surface concluding thus that they have unstrained monolayers, which explains the unaffected E_{1g} peak.

In the PL spectra, an increase of the trion peak is presented for some substrates. It was explained by doping effects through charge transfer from the substrate charging the neutral A excitons. This effect is also presented as the one responsible for the A_{2g}^1 changes.

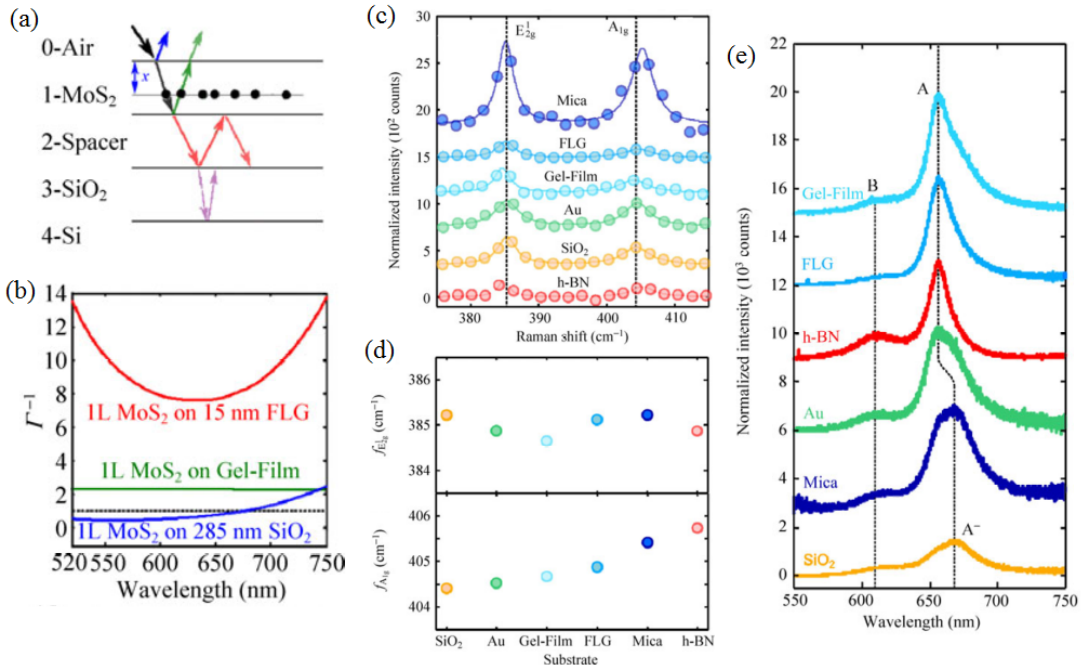

Figure 16 – (a) Interface representation in which 2-Spacer corresponds to the substrate to be studied. (b) Wavelength dependence of the enhancement factor of some substrates. (c) Raman spectra of the MoS_2 monolayer over different substrates and (d) the changes on its active Raman modes E^1_{2g} (top) A_{1g} (bottom).(e) Photoluminescence spectrum of the MoS_2 monolayer in each substrate. Taken from [4].

The study of PL reveals also that all the substrates investigated improve the monolayer emission in comparison with the SiO_2 substrate.

CHAPTER 3

Experimental Setup

3.1 Sample fabrication

When the mechanical exfoliation method is used to produce samples on GaAs, a low contrast between a few layer flake and the substrate is observed. Single layers of TMDs are difficult to find by this way. Thus, identifying the single layer before the transference increases the probability of finding the monolayers after it. In this way, the all-dry viscoelastic stamping method is used: an exfoliated tape is pressed against a gel film[1] and then it is peeled off slowly [76]. This will allow an improvement of the optical contrast for mapping the sample in the microscope, in search of TMD monolayers. After identifying all possible monolayers in the gel, a Hg lamp is used to see its fluorescence under the microscope. If strong fluorescence occurs, there is a high probability of having found a single layer or even a bilayer for WSe_2. Photos are taken of each flake in order to know its exact position on the gel. In Figure 17 it is presented a schematic illustration of the fabrication process.

Then, the GaAs substrate is cleaved in small squares of $\sim 6\ mm$ by side and ultrasonically cleaned by five minutes on acetone and isopropyl alcohol, in this order. Subsequently, gel film samples are aligned with the substrate and softly pressed against it. Without separating them, the junction is put on the hot plate at $80°C$ for ten minutes. Then, the gel is peeled off slowly to improve the transference of the flakes. Previously identified monolayers should be found by comparing the flakes with the photos taken from

[1] It is possible to use ©Gel Film available on its site, or by preparing it. We fabricate it in the clean room with ten parts of silicone SYLGARD 184 BASE by one of SYLGARD 184 CURING AGENT mixing it well and leaving it to dry over three days.

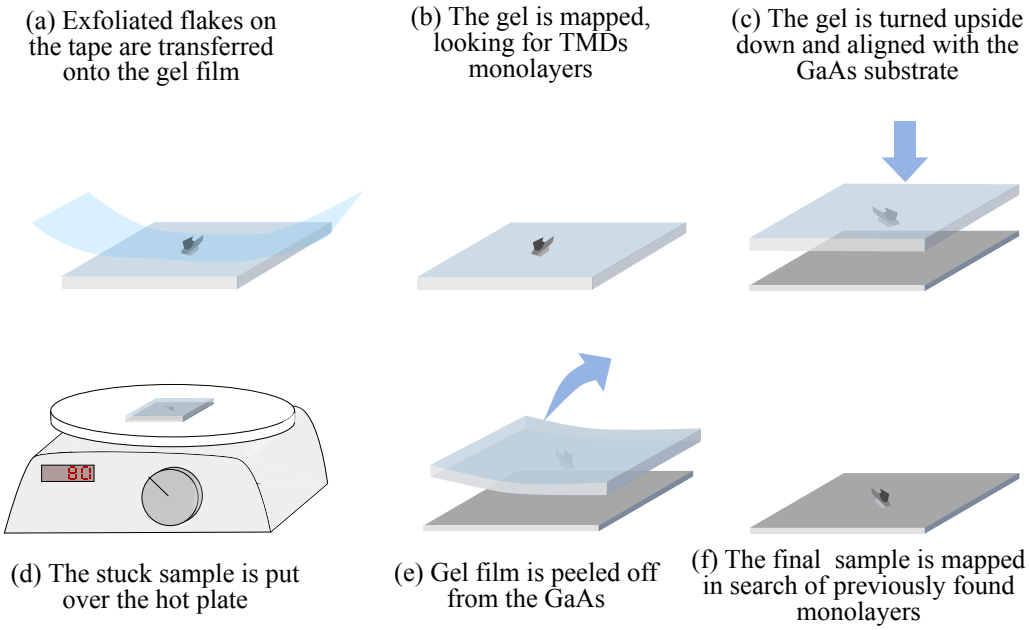

Figure 17 – Schematic illustration of the sample fabrication process.

gel[2]. Thereby, new photos of single layers on the substrate should be taken to determine their exact position for their subsequent measurement. Figure 18 presents the optical images of a flake in each step of the fabrication process.

After using the reference photos from the gel and identifying the flake or the region in which the single layer should be, it is possible that it apparently has not been transferred. Due to the low contrast, the optical image cannot be used to define if the transference process has been successful. Then, fluorescence by Hg lamp is used again for the WS_2/GaAs junction, revealing if there is single layer emission. Moreover, for MoS_2 and WSe_2 on GaAs, monolayer fluorescence is suppressed, which gives us the first hint that charge transfer occurs in these cases, from the TMD to the substrate. Owing to this, to locate the single layers in these cases we have to use a dark field filter, which provides us an image of the scattered light by any edge or defect in the surface.

Figure 19 presents the refractive index of some representative materials. It is possible to see that GaAs and MoS_2 [3] have close values of the refractive index in the visible range, explaining the low optical contrast at the monolayer limit. On the other hand, it is possible to see the significant difference between the SiO_2 and the TMDs refractive indexes, which can explain why monolayers are much easier to identify on this type of substrate.

[2] Transference process does not necessarily transfer the entire flakes, they can appear in a fragmented way or even remains on the gel.

[3] As well as the other TMDs, by comparison with Figure 6.

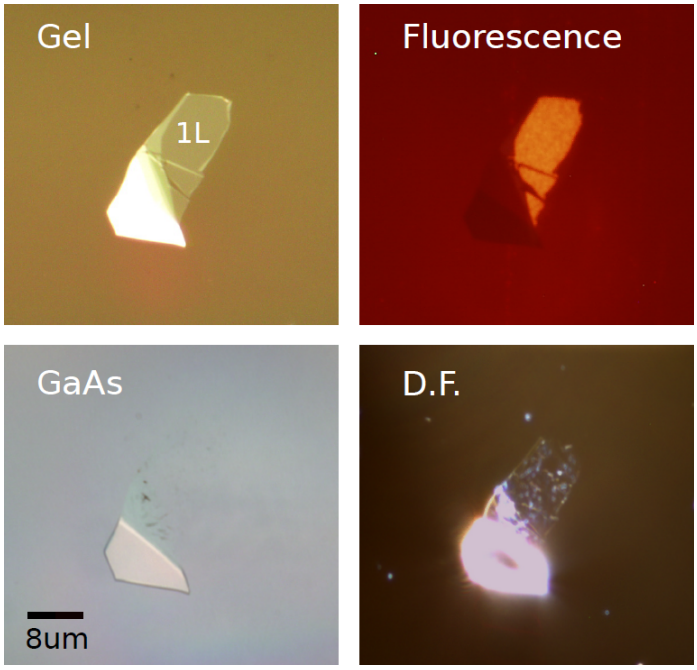

Figure 18 – Single layer identification process. Optical image of a WSe2 sample over gel film (top left) and after transference on a GaAs substrate (bottom left). Fluorescence of the same sample on gel (top right) and optical image using a dark field filter of the sample on GaAs (bottom right).

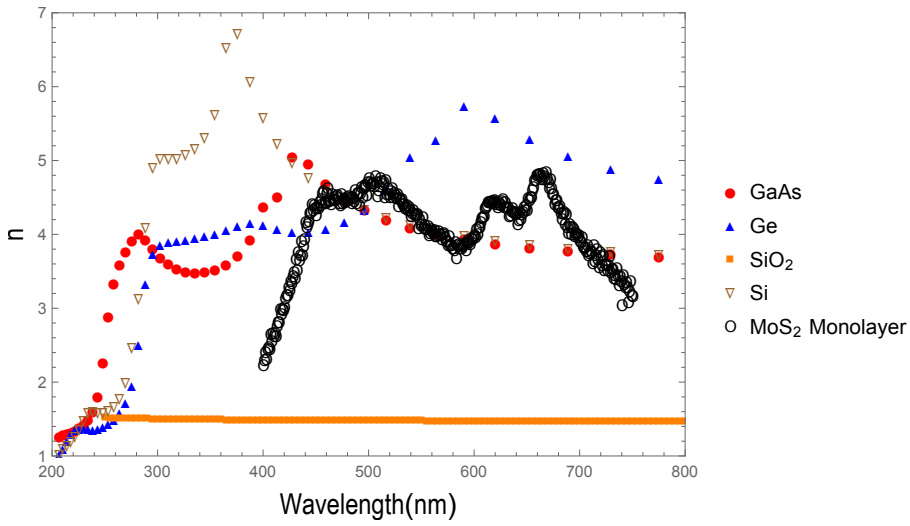

Figure 19 – Refractive index for some substrates and a the MoS_2 monolayer. Data taken from [77] [78] [79] [80].

3.2 Raman Spectroscopy

Sample characterization can be done in many possible ways, one of them is Raman spectroscopy. This powerful optical characterization technique allows us to study the

vibrational modes of the material. In that, the photons from a laser beam excite the molecules in a sample, driving them up to a virtual state for its subsequent decay in one of three possible ways. First, molecules can decay to the same initial state, by emitting a photon with the same energy of the incoming beam (Rayleigh scattering). Second, they can decay to state with energy higher than the initial state by emitting less energetic photons than the incoming ones (Stokes scattering). Third, the molecules can go to a less energetic state than its initial condition, by emitting photons with an energy higher than the energy of the incoming beam (anti-Stokes scattering). In the latter two cases, the difference in energy is given by the emission (Stokes scattering) or the absorption (anti-Stokes scattering) of a phonon of the scattering material. Usually, measurement of the intensity of these emissions is done as a function of the difference between the wave number of the excitation beam and the emitted light:

$$R_s = \left(\frac{1}{\lambda_{ex}} - \frac{1}{\lambda}\right) \tag{3.1}$$

with R_s the Raman shift in cm^{-1}, λ_{ex} is the wavelength of the excitation beam and λ is the wavelength of the scattered light.

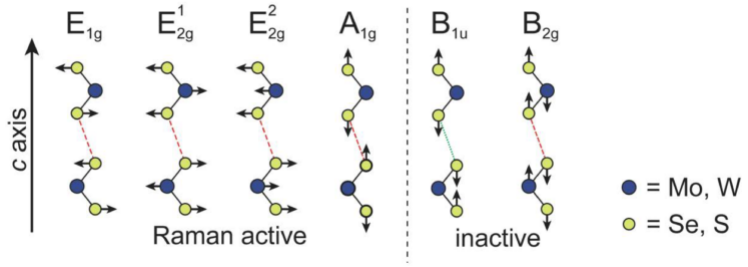

Figure 20 – Schematic illustration of the main Raman modes of the transition metal dichalcogenides [81].

Figure 20 shows the Raman modes of the TMDs in a bilayer representation. When the light interacts with the molecules in the lattice, the vibration modes can affect the charge distribution. Those modes which have oscillating polarizability in the normal direction will be called the active Raman modes and otherwise, the inactive ones. In particular, for the single layer case, the two main active modes will be the E^1_{2g} (in-plane oscillation) and A_{1g} (out of-plane oscillation) detected as two thin peaks in the Raman spectrum.

The main setup for optical spectra measurements consists of a light exciting source (laser), a diffraction grating/monochromator and a sensor. The photons emitted by the sample arrive at the diffraction grating which separates them by their wavelength and also

determines the range of spectrum that will be analyzed. Depending on its number of lines per millimeter, the grating can provide better resolution in the spectrum by reducing, in consequence, the range of wavelengths on the spectrum. Once the photons pass by the grating, they are detected by a sensor (CCD) which transforms the light into electrical signals that are converted by a software into a spectrum.

For Raman spectroscopy, we use the WITec [82] *alpha 300A* experimental setup available in the laboratory LCPNano at UFMG. The samples were excited with a 532 nm wavelength laser with a 0.8 mW power[4]. The Table 3 presents the position of the two active Raman modes in the monolayer of the different TMDs.

	Raman mode (cm^{-1})	
TMD	E^1_{2g}	A_{1g}
WS_2	357	418
MoS_2	384	404
WSe_2	-	249
$MoSe_2$	286	239

Table 3 – Experimental values of the active Raman modes in TMD monolayers [52].

3.3 Photoluminescence Spectroscopy

As explained in the last chapter, the photoluminescence spectrum measurement allows us to study the electronic transitions produced in the sample. For the measurements of spectra at room temperature, the same system used for Raman spectroscopy, the UFMG WITec equipment was used[5]. The flakes are localized and measured with a 100x objective in order to reduce the spot size and improve the control about which point (region) in the sample is excited.

Two kinds of spectral measurements were taken, single spectrum and spectral maps. In the first one, the emissions of a specific point of the monolayer are analyzed. To reduce the noise, the exposition time of the CCD as well as the number of acquisitions are pre-defined. In the second one, a region of the sample is defined, along which a set of single spectra will be taken to construct the spectral map of the region. Thus, the parameters as the number of spectral points in the x and y direction should be defined as well as the CCD exposition time and number of acquisitions of each single spectrum.

High reliability of the measurements is provided by the WITec system, due to its high optical precision as well as its CCD quality. However, due to its configuration, it is

[4] Warning: a high laser power can damage the single layers. This power is enough to see weak emissions without damages. Nevertheless, short exposition time (few seconds or less) is recommended.

[5] Some measurements were done in a similar equipment but in the CTNano-UFMG laboratory.

physically impossible to place a cryostat in it in order to make low temperature or vacuum measurements. In this way, it was decided to adapt a low-temperature setup available on the Semiconductor Laboratory, discussed below, for photoluminescence measurements below room temperature.

3.3.1 Low temperature Photoluminescence

For the low-temperature measurements, the setup presented in the Figure 21 was used. In the diagram, it is possible to see the optical path followed by the excitation laser and how it reaches the sample, placed in the cryostat, for its subsequent reflection up to the spectrometer. In the inset we can see a photo of the setup centered in the cryostat region which is placed in a different plane of the rest of the optical system; the latter with the purpose to give more stability to the mapping system as well as to the cryostat. The objective is placed over an electronically controlled piezoelectric (P) which allows us to make spectral maps over a region of the sample by using its three axes. To orientate the laser beam to the sample, the M3 mirror is placed above the objective (inset Figure 21).

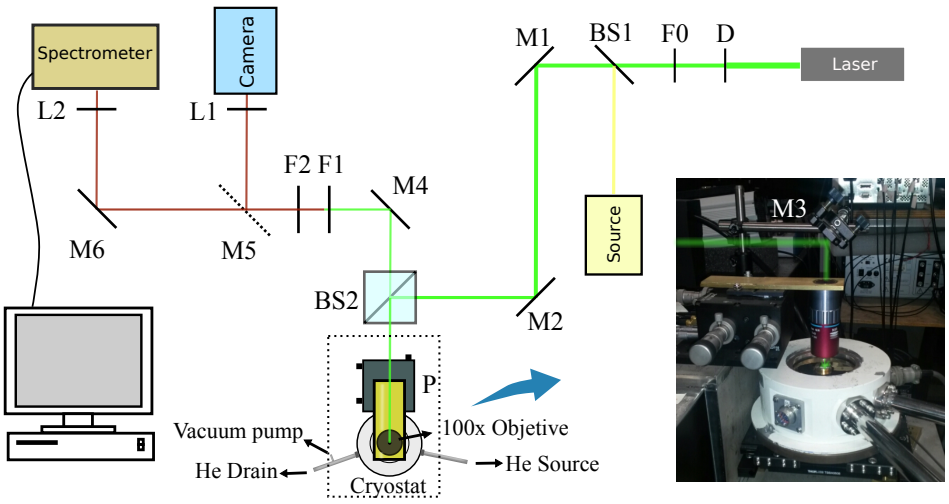

Figure 21 – Diagram of the experimental setup for low temperature measurements. The inset shows a photography of the cryostat with the objective and the mirror M3 above it.

To control the intensity and the spot size, an intensity filter ($F0$) and an iris (D) were used to prevent possible damages on the sensors[6]. The F1 filter with a 568 nm value is a high-pass filter used to suppress the laser line, allowing us to focus on the light coming from the sample. Owing to the high intensity of the GaAs luminescence peak, an additional filter (F2) is needed specifically at low temperatures, where overlapping with the TMDs PL is highest. Due to the separation of the PL peaks of the GaAs (830 nm) and the MoS_2

[6] It is not considered a risk for the single layers due to the low laser power ($\sim 0.5mW$).

(678 nm) or WS_2 (640 nm), a low-pass filter $F2 = 750\ nm$ is enough to mitigate the substrate effect. For the WSe_2 case, whose photoluminescence (750 nm) is closer to the GaAs value, a low-pass filter $F2 = 810\ nm$ is used.

To find the TMDs single layers, the white collimated light *source* is turned on and the beam splitter BS1 drives the beam to the optical path of the laser. By placing a mirror (M5) we direct the image of the sample to the camera. Once the monolayer is located, the lamp is turned off and M5 mirror is removed[7] in order that the optical path continues up to the spectrometer. Two 100 mm convergent lenses L1 and L2 are used to focus the light beams into each sensor. An Ocean Optics USB2000 spectrometer with an internal (and fixed) 600 lines/mm grating is used. The advantage of this spectrometer is its high spectral range, although the spectral quality is affected owing to the short optical path and low resolution grating.

To realize the measurements, first conductive silver paste is used to fix the sample to the cryostat and then the monolayer is found by using the system. Thereby, the cryostat window is placed and vacuum is made by using the Edwards pumping station XDS10. After a stable inside pressure of the order of $\sim 10^{-5} Pa$ is achieved, He flux is opened and temperature is monitored until the desired value is reached.

[7] A Thorlabs flip mount adapter is used to maintain the system alignment.

CHAPTER 4

Results - TMDs on GaAs

The use of the transference method described before does not imply a full transference of the flakes or bulks; the transference can happen in a partial way or the flakes may even remain on the gel. Also, the transference process can be seen as a new exfoliation of the TMDs. The Figures 22 - 24 present the samples used in this work. Low contrast is appreciated in the GaAs substrates demonstrating the difficulty to see the single layers with the optical microscope.

For the MoS_2 samples, in Figure 22, the images on the GaAs with the dark field filter show a transference of most of the previously identify monolayers. In the undoped substrate the monolayer does not seem to have been transferred, however the sample is studied to see if there occurs a new exfoliation transforming the few layer (FL) region in a single layer one. In the n-GaAs substrate, on the other hand, the majority of the single layer seems to be transferred, but in a rough way.

For the WS_2 flakes, Figure 23, the undoped and p-GaAs substrates show a partial transference of the TMD bulk as well as the monolayers. The presence of bulk regions close to the single layers facilitates their location for the subsequent measurement. In particular, the p-doped case is challenging owing to the single layer being isolated of any bulk. This monolayer, in other conditions, would go unnoticed. In contrast, the flake on the n-GaAs substrate is one of the full transference cases, making it easy to find.

Finally, the WSe_2 on GaAs, Figure 24, is the set with the best transferences obtained, almost the entire flakes (bulk and monolayer) were transferred.

Fluorescence of the flakes, in the gel, is not enough to determine if the flakes are in fact monolayers, thus, characterization should be done through Raman spectroscopy,

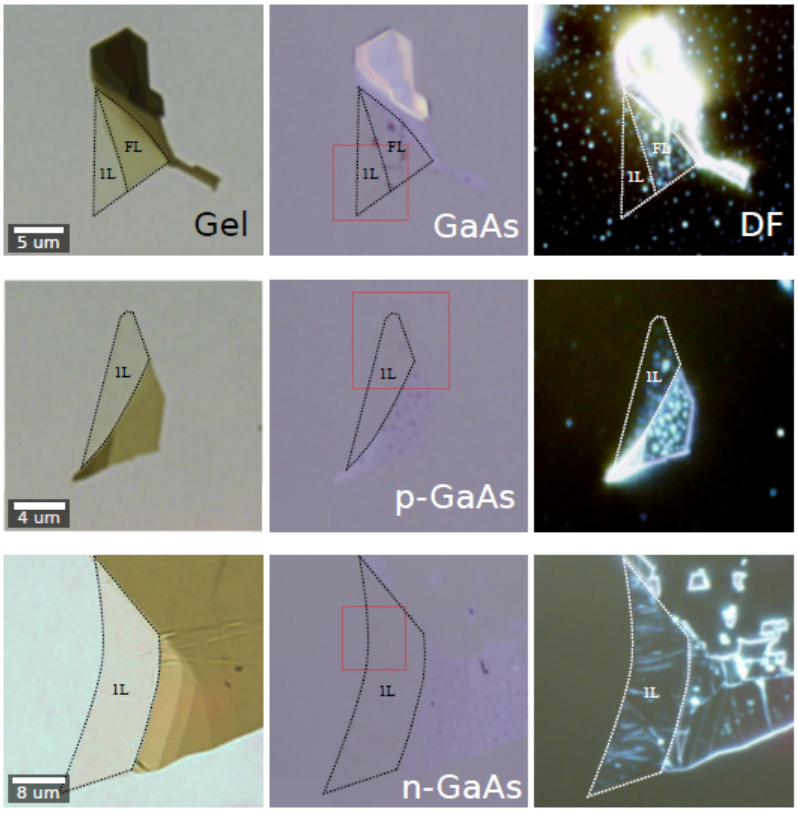

Figure 22 – Set of MoS_2 samples on the gel (left), on the substrate (middle) and the dark field filter image of the flake (right). The monolayer areas (1L) and few layer (FL) are represented with dotted lines.

which will be presented in the next section.

4.1 Raman spectrum

The Raman emission, as mentioned before, provides information about the vibrational modes of a material, which can change depending on the number of layers. In particular, the relative positions of the E^1_{2g} and the A_{1g} Raman modes of MoS_2 will provide information about the number of layers in the crystal. This distance, for the monolayer case takes values between 18 cm^{-1} to 19 cm^{-1} [83, 84].

Figure 25 displays the Raman spectra of the MoS_2 monolayers on the different substrates. Peak differences of 19.0, 18.1 and 17.8 cm^{-1} in the undoped, n-doped and p-doped substrates respectively, are found. This fact reveals the unambiguous single layer character of the samples. The inset also presents an expanded view of the spectra, with the respective substrate peaks at $\sim 267 cm^{-1}$ and $\sim$ 290 cm^{-1} for the doped cases and 292.4 cm^{-1} for the undoped one.

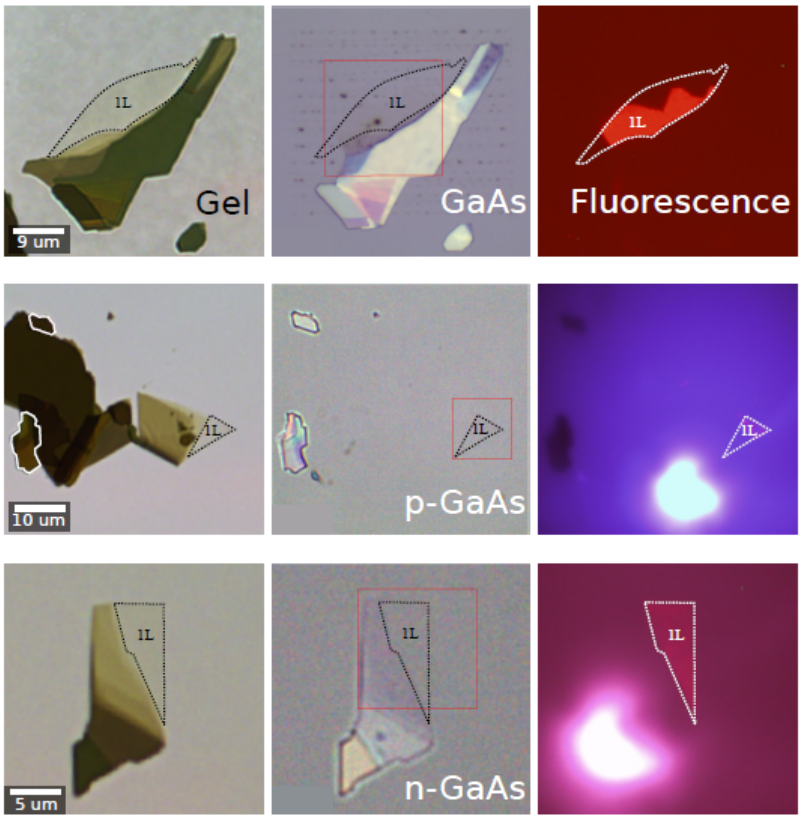

Figure 23 – Set of WS_2 samples on the gel (left), on the substrate (middle) and the fluorescence image of the flake (right). The monolayer areas (1L) are represented with dotted lines.

These results are obtained after making three single acquisitions of ten seconds each in the single layer regions represented in Figure 22 for both doped cases. For the undoped substrate, despite the invisible state of the previously identified monolayer, after measurements in that region, a single layer spectrum (presented in Figure 25) is obtained. It shows the difficulty in the single layer identification even with the use of the DF filter and underlines the importance of the monolayers on the gel film.

The WS_2 single layer features of the Raman spectra, as studied by *Berkdemir et al.* [85], will exhibit a dependence on the wavelength of the excitation laser. For example, a richer spectrum, with second-order peaks, is obtained with $\lambda_{exc} = 514.5\ nm$, while a more clear signal of the two main Raman modes is observed with $\lambda_{exc} = 488\ nm$. Due to these changes, WS_2 single layer determination will also depend on the laser line. For $\lambda_{exc} = 514.5\ nm$ the spectrum is dominated by three main peaks: the first is the strongest second order Raman peak associated to a longitudinal acoustic mode ($2LA$). This mode is produced by collective in-plane movements of the atoms in the lattice. The second is the E^1_{2g} peak which, in this case, will be overlapped with the $2LA$ peak but also resolvable. The third is the A_{1g} peak, which in the monolayer case will present an intensity of about a half of the $2LA$ mode. The latter will be the determinant criteria of the single layer

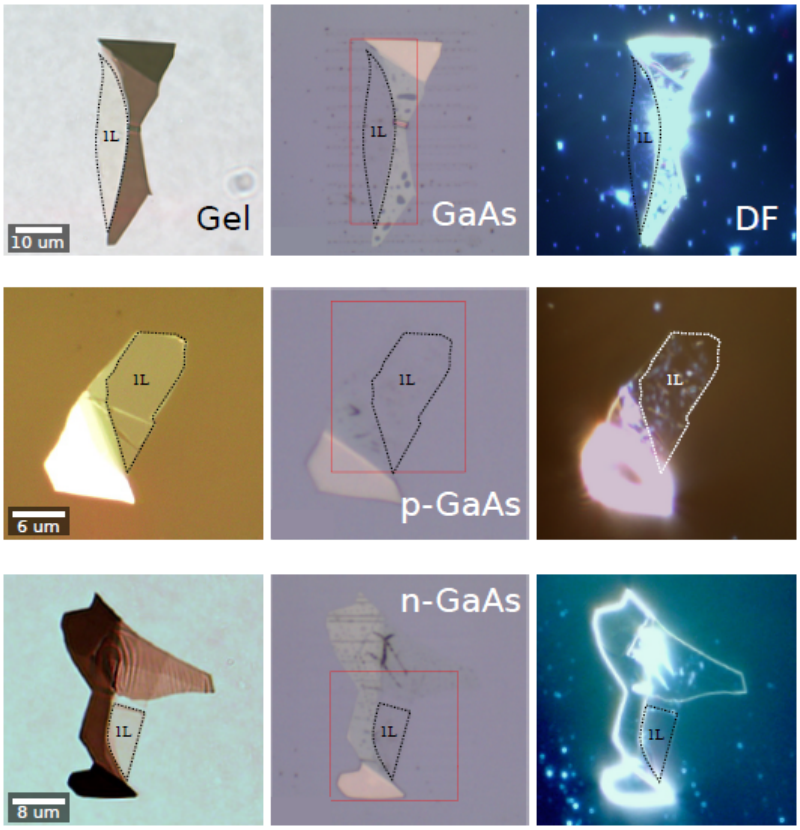

Figure 24 – Set of WSe_2 samples on the gel (left), on the substrate (middle) and the dark field filter image of the flake (right). The monolayer areas are represented with dotted lines.

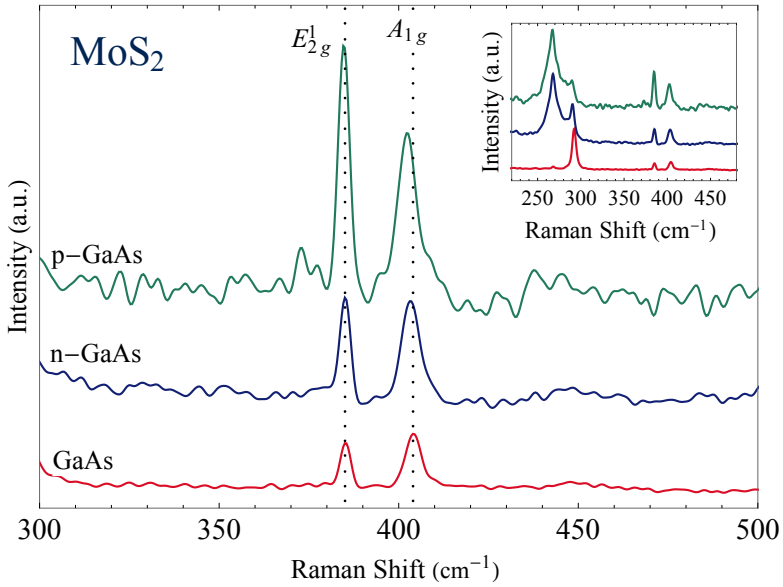

Figure 25 – Raman spectra for MoS_2 in each GaAs substrate. Dotted lines: 385 cm^{-1} and 404 cm^{-1}. $\lambda_{exc} = 532\ nm$.

condition. For $\lambda_{exc} = 488\ nm$, the authors report a linear increase of the intensity with the number of layers up to three layers and then a decrease from four layers to the bulk. The dominant Raman modes in these spectra will be the two active modes of the TMD. In both cases an additional criteria for the monolayer identification is observed: a redshift of the A_{1g} mode produced by the less intense restoring force caused by the van der Waals interactions. This is the same phenomenon observed for MoS_2 [83]. For WS_2, the E^1_{2g} mode will be close to 355 cm^{-1} without thickness dependence, and the A_{1g} will be placed close to 417 cm^{-1} for the monolayer case and close to 420 cm^{-1} for the bulk.

For the Raman spectrum measurement, a laser line of $\lambda_{exc} = 532\ nm$ was chosen due to the deterministic intensity relation between the $2LA$ and A_{1g} modes. However a low resolution was observed for the doped substrates. Then, an increment in the acquisition time to 20 seconds was made to improve the spectra, without significant changes. The Figure 26 (left) presents the Raman spectrum measurements in each GaAs substrate. The undoped GaAs substrate shows the expected peak intensity relation and all the second order reported modes [85] for the $\lambda_{exc} = 514.5\ nm$, confirming the monolayer condition of the sample.

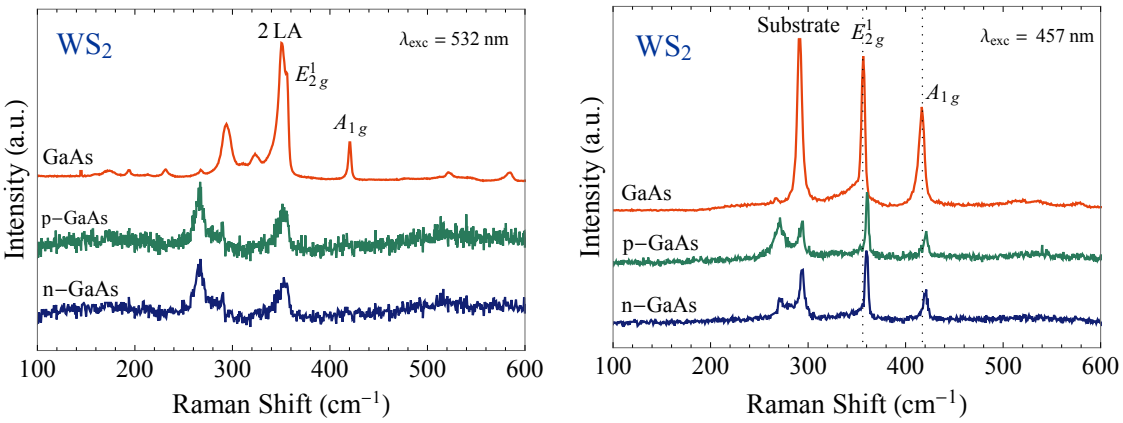

Figure 26 – Raman Spectrum for WS_2 with a 532 nm (left) and 457 nm (right) wavelength excitation lasers.

On the other hand, the determination of the monolayer limit for the doped samples required the use of a different laser line of $\lambda_{exc} = 457\ nm$ to use the criteria of the A_{1g} peak displacement to determine if the selected flakes are monolayer. The measured spectra are presented in the Figure 26 (right). As expected, strong TMD main modes are observed, similar to the reported case of $\lambda_{exc} = 488\ nm$. The positions of the peaks agrees with those reported for the monolayer case giving us the certainty about the flakes number of layers. Nevertheless a difference in the intensity relation of the two modes is observed. Thus, additional spectra are taken for the bulk and a few layer region to observe how the spectra changes in each case. Figure 27 presents these results and confirms the A_{1g} redshift when the single layer dimension is achieved. In addition a high intensity is observed for the few layer spectra, it is explained as an interference effect produced by the substrate and layer

interfaces [85]. Finally, the different relation of intensity between the A_{1g} and E^1_{2g} modes with the reported values can be due to the difference in the laser lines. Figure 27 shows the spectra in the undoped substrate; analogous results are observed for the doped cases.

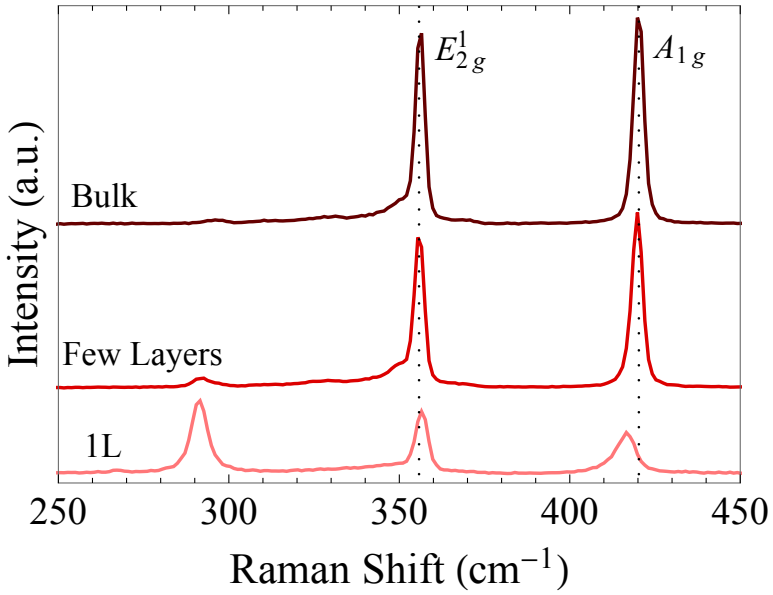

Figure 27 – Raman spectra for different thicknesses of WS_2 over an undoped GaAs substrate and a 457 nm wavelength laser excitation. Dotted lines: 355 nm and 417 nm. Few layer spectra is presented with half of its intensity.

In the WSe_2 case, the Raman monolayer spectrum will differ from its bulk counterpart by three representative features: a high intensity emission of the A_{1g} mode close to 250 cm^{-1} with no clear signal of the E^1_{2g} mode[1], a broad $2LA$ peak close to 260 cm^{-1}, and the absence of a tiny peak at 309 cm^{-1} [81, 86]. The Raman spectra of the WSe_2 monolayers is presented in Figure 28. All three features are observed with less intense emission for the doped cases. Differences are observed in the substrate peaks, the undoped GaAs mode exhibits a comparable intensity to that of the A_{1g} mode whereas the doped GaAs (p and n) Raman modes are almost unobservable in comparison with the WSe_2 emission.

	MoS_2		WS_2		WSe_2	
	E^1_{2g}	A_{1g}	E^1_{2g}	A_{1g}	E^1_{2g}	A_{1g}
GaAs	385.1	404.1	356.5	416.4	-	249.1
n-GaAs	385.1	403.2	360.1	421.2	-	250.2
p-GaAs	384.7	402.5	359.5	420.0	-	249.3

Table 4 – Measured values of the active Raman modes of TMD monolayers in (cm^{-1}).

[1] The observed signal can be produced for either unresolvable peaks or by a degenerated condition. Solid evidence is not presented in the literature so far.

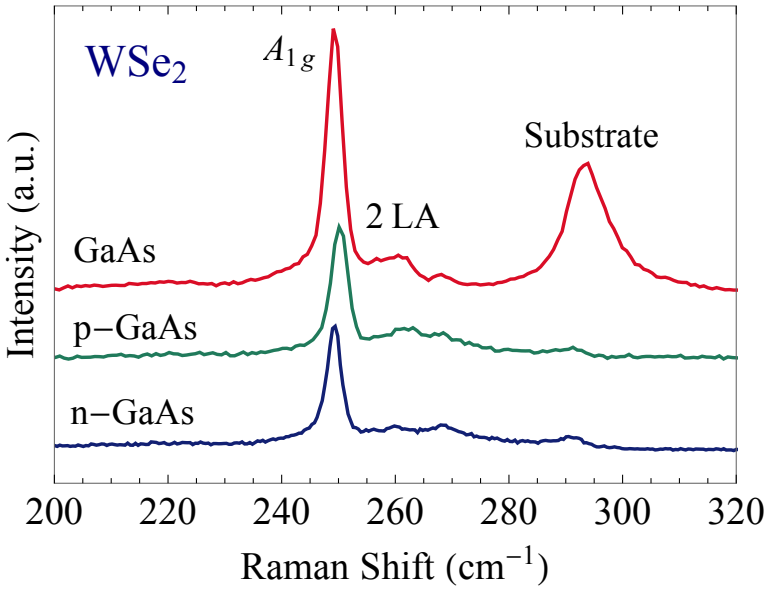

Figure 28 – Raman spectra for WSe_2 in each GaAs substrate for a 532 *nm* wavelength laser excitation.

4.2 Photoluminescence

The main physical features involved on the PL spectra of the TMDs were previously discussed in section 2.4. Here, we will present the main results of the different measurements. An initial clarification about emission intensity must be done: just room temperature measurements were taken under equal conditions (laser power, acquisition time, system alignment), thus it is natural to expect a direct comparison between samples in that case among different substrates, nevertheless TMD monolayers are materials subjected to many variables (as mentioned in chapter 2) such as defects on the TMD lattice, defects on the substrate, inhomogeneous transference of the monolayer to the substrate leading to roughness and thus, an inhomogeneous charge transfer. On this way, when one chooses an arbitrary point in the sample to make the measurements, it is not guaranteed that the measurements will describe the monolayer general behavior. On that way, a more objective intensity analysis could be realized by taking spectra in different points of the monolayer from different samples and constructing a complete statistics. Owing to this latter, a spectral intensity comparison will not be done among substrates.

Low temperature spectra were taken under different conditions (acquisition time, laser power) due principally to the too intense GaAs PL emission. Even with a filter for the laser beam, the broad linewidth of its PL and the blue shift at low temperature, allowed the pass of an intense PL substrate tail. In addition, PL from some TMDs were too weak in comparison to that background, making it dangerous for the spectrometer CCD detector that can not withstand a long exposure time measurement. Nevertheless an

enhancement in the intensity is observed in all the samples at low temperature. This is commonly associated with a decrease of the non-radiative processes at low temperature condition and is also described as [22]

$$I(T) = I_0 \frac{k_r(T)}{k_r(T) + k_{nr}(T)}$$

where I_0 is the approximated intensity at 0 K, k_r and k_{nr} the radiative and non-radiative recombination rate [87]. In addition, low temperature increases the band gap in semiconductors [88] producing higher energy transitions.

Due to the high and overlapped intensity of emission of the GaAs substrates, all the PL spectra were filtered by subtracting from them the substrate PL and then cleaning the signal with a low pass filter in ©*Mathematica*[2]. Finally, the signal was fitted by the individual contributions of each quasiparticle in order to facilitate the spectral analysis (see Appendix A).

The PL of the MoS_2 monolayers at room and low temperature is presented in Figure 29. Main emissions in the room temperature spectra are produced by the A and B excitons with the higher contribution from A exciton since that exciton require less energy to be formed as is widely reported in the literature. The spectra were fitted by a sum of Voigt lineshapes (for excitons A and B) and an asymmetric Voigt line (for the trion). We find that the trion can only be fitted by an asymmetric lineshape, which can be understood, as discussed below.

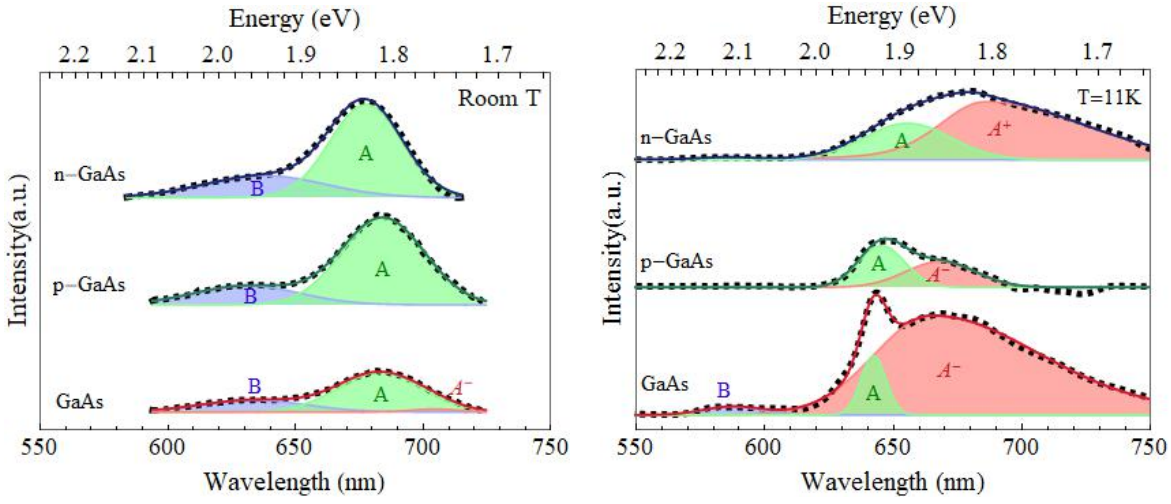

Figure 29 – PL spectra for MoS_2 at room temperature (left) and T=11 K (right). Experimental data (dashed line) and fits (continuous line).

To analyze the PL at low temperature it is useful to determine if charge transfer occurs and in what way. When the junction of MoS_2 and GaAs is produced, charges can

[2] https://www.wolfram.com/mathematica/

transit from one material to the other depending on the band structure offset. Figure 30 presents the band alignment for each substrate by representing the Fermi level (FL) in green (dashed line). The actual band offsets for the system MoS2/GaAs is still not firmly established. We follow the proposal of *Lin et al.* [1], that will help us to explain the obtained results.

We can see that charge transfer must occur from the negatively and undoped substrates to the monolayer owing to the difference in the Fermi level on each material. Once the Fermi level reaches the equilibrium in the junction, the density of electrons in the TMD will be higher. When the laser beam excites electrons from the valence band they will achieve the conduction band of the monolayer but part of them will be transferred onto the substrate owing to the energy difference. This behavior will be more prominent in the n-GaAs substrate than in the undoped one. Now, for the holes in the valence band, for n-GaAs, we can see that their energy minimum will be at the MoS_2 monolayer, while for the undoped one, holes are transferred into the substrate. These transfer will favor the dissociation of the excitons in the negatively doped substrate and the complete transfer of them to the undoped one.

On the other hand, for the positively doped GaAs, photo-excited electrons in the monolayer will remain in the dichalcogenide, while the associated holes in the valence band will have an increased probability to be transferred to the substrate owing to the energy difference in the interface. It means that in this case, excitons will have an increased rate of dissociation.

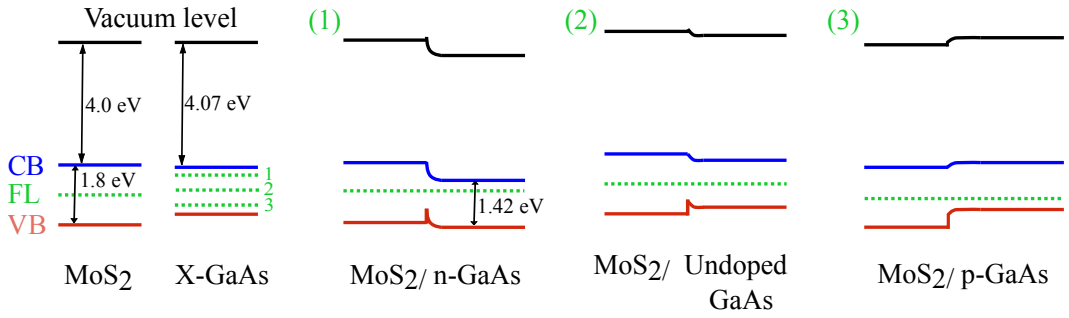

Figure 30 – Proposed band alignment diagram of the MoS_2/GaAs junction.

According to our last analysis, photoluminescence should be less intense for MoS_2 on GaAs than for MoS_2 on an insulator or a SiO_2 substrate. However, it is difficult to quantify, from an experimental point of view, which of the substrates will have the more important mitigating effect on the PL, because of the many variables involved. From a qualitative point of view, we observe a less intense emission, in all three samples, compared to those obtained in a conventional SiO_2. However, we can make a ratio between the intensity of the exciton peaks I_B/I_A to obtain information about the different effects of the substrate. Since exciton B requires higher energy to be created, it has less probability to

be formed in a system with a low charge density. For this reason, it is more common that they emerge and remain in defects on the single layer which trap the exciton. Furthermore, I_B/I_A relation can be related to the number of defects in the monolayer [89].

	Room Temperature	Low Temperature	
Substrate	I_B/I_A	I_B/I_A	I_T/I_A
n-GaAs	0.23	0.05	1.59
GaAs	0.30	0.14	1.68
p-GaAs	0.19	-	0.62

Table 5 – Relative intensities of the emission peaks in the PL spectrum of MoS_2 on different GaAs substrates.

We obtain the intensity ratios of 0.23, in the negatively doped substrate, 0.30 in the undoped one and 0.19 for the positively doped. It implies that many of the luminescence that we can see is associated with excitons that remain trapped in the single layer, especially in the undoped substrate. These defects should also be responsible for most of the emissions coming from the exciton A. Furthermore, we believe that due to the small energy difference in the conduction and valence band between the materials, in the junction of the undoped sample, the dissociation of excitons is smaller and enables that some of them remain on the MoS_2 flake.

At low temperatures, non-radiative processes decrease and it is possible to obtain more information from the PL. From our results in Figure 29 we observe a prominent, unexpected, trion emission in all the samples. However, since charge transfer occurs, low charge density was expected. Trion emerging, on the other hand, is a signal of high charge density. In Table 5 we present the relative peak intensity in each sample. We observe that the same pattern obtained for room temperature is maintained: low relative intensity for the positively doped sample emission, and the highest value for the undoped one. Thus, we can say there is a high hole transfer from the MoS_2 monolayer to the p-GaAs substrate that dissociates the excitons and mitigates the photoluminescence of the sample. At low temperature, excitons and charges remain (defect assisted) on the monolayer and form trions, most of them negatively charged.

The negatively doped substrate exhibits the second highest charge transfer, in this case, of electrons from the TMD to the substrate. At low temperature the high density trapped in the defects gives rise to an intense trion peak; we believe most of its emission coming from positively doped excitons, according to our proposed band offset.

Finally, the undoped substrate shows the most intense emission, which suggests a higher density of defects that capture the excitons and favors the emerging of trions at low temperatures. Some of these defects can be observed all around the undoped substrate in the dark field filter in Figrure 22 for MoS_2 as well as in the WS_2 and WSe_2 samples. It

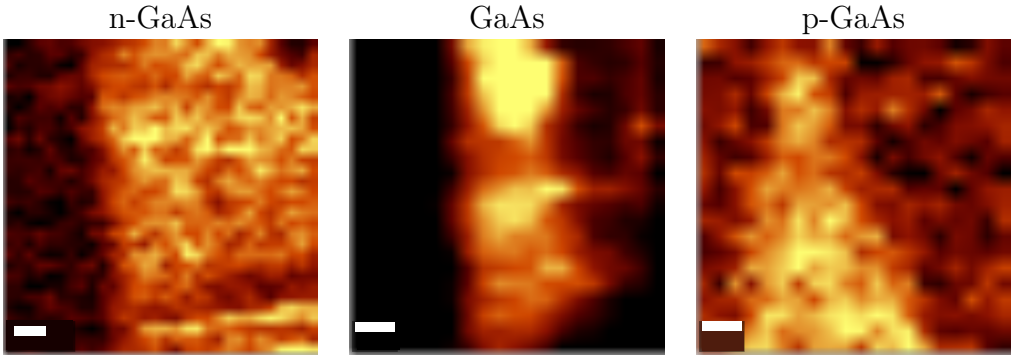

Figure 31 – MoS_2 PL maps of the red areas shown in the Figure 22. The scale bar is 1 μm in all panels; the PL maps do not have the same color scale.

could be due to how the substrate is produced [3], or its cleaning procedures. New cleaning procedures could help to reduce this fact. In the same way, the photoluminescence map of this substrate exhibits less uniform intensity (Figure 31), in agreement with our defect hypothesis.

It is worth noting that the trion emission presents a long low energy tail, which gives rise to its asymmetric lineshape. It is produced by its recombination pathway: the trion decay can be understood as a two-step process: first an electron is unbound from the trion and then the recombination of the electron-hole pair occurs. When the electron leaves the trion, in general, it will be released with a non-zero momentum, producing a less energetic photon emission owing to the less energetic electron-hole pair [22].

Photoluminescence maps were taken over the areas in the samples marked by red squares on Figure 22, and are presented on Figure 31. A small PL contribution of the as-called few layer region in the undoped substrate is observed, probably produced by strain in the wrinkles. The doped substrates, on the other hand, present a more homogeneous intensity distribution, associated, as mentioned before, to a minor quantity of defects on the monolayer or in the interface. A better contrast can be seen on the undoped substrate, which could be related to the small line width of the pristine GaAs PL in comparison with the doped ones (*See Appendix A*).

As expected from the fluorescence process, a high PL intensity was observed in the WS_2 samples. In Figure 32 we can see the PL map of the sample on the undoped substrate which exhibits two intense regions, one in the middle, over a defect (visible in Figure 23) and the second over an edge. The first one suggests a strain over the single layer producing a PL enhancement. The second one is probably a non-full contact region with the substrate which also leads to a more intense luminescence. The latter phenomenon can also be observed in the n-doped GaAs substrate which has an intense emission in the middle region. Finally the p-doped sample presents two regions with a high intensity,

[3] Wafer Technology http://www.wafertech.co.uk/products/gallium-arsenide-gaas

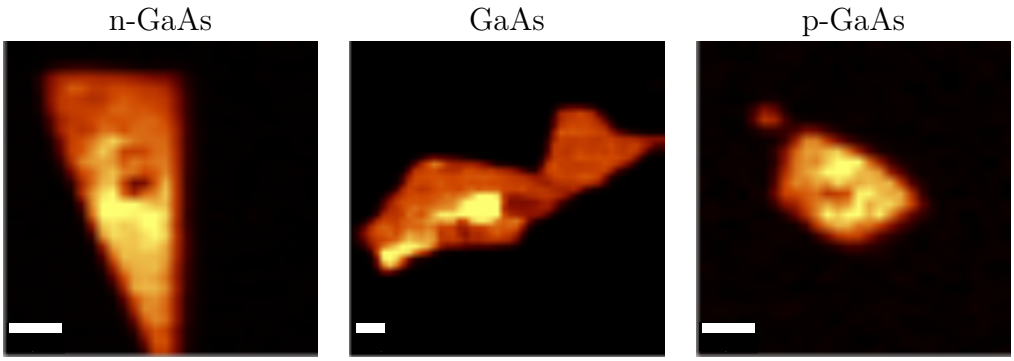

Figure 32 – WS_2 PL maps of the red areas shown in the Figure 23. The scale bar is 2 μm in all panels; the PL maps do not have the same color scale.

produced by local defects of the substrate or the TMD.

Three important features are observed in the spectra of Figure 33: a trion dominated emission, an intense luminescence of the undoped sample and a different blue shift of the low temperature measurements. Explanation will be developed through a band structure analysis but, unlike the MoS_2 band offset, for WS_2 as well as for WSe_2 there have not been any band alignment reports for a GaAs heterojunction, in our knowledge. However, due to the fact that TMDs are van der Waals bounded layers and the lattice parameters will not be affected by the substrate, we can estimate the band alignment of WS_2 (and WSe_2) with GaAs by transitivity, using band offset studies among MoS_2/WSe_2 and MoS_2/WS_2.

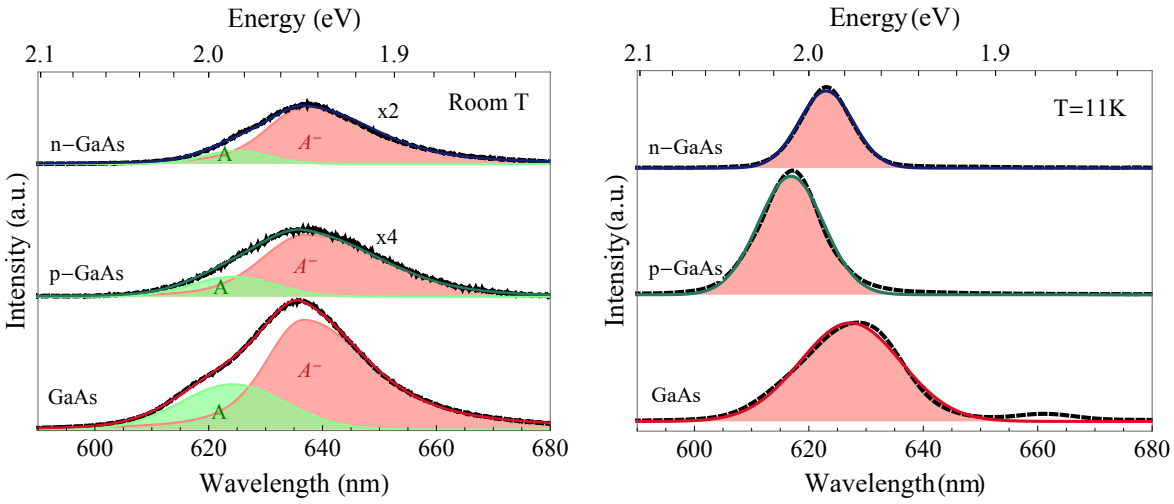

Figure 33 – PL spectra for WS_2 at room temperature (left) and T=11K (right). Experimental data (dashed line) and fits (continuous lines).

It could take a long time and much research until an agreement is established for the relative energy values of band alignment in heterojunctions. Thereby, significant differences can be found in the literature, depending on the analysis method so much as theoretical as experimental. In this way, the selection of an exact energy difference between bands will have a subjective component. However, all reports agree on one thing: WS_2

and WSe_2 bands will be displaced to higher energy value compared to the MoS_2 band structure [90–93]. For WS_2 we will propose the band offset shown in the Figure 34.

Due to the large Fermi level of the WS_2, a static charge transfer will occur from the single layer to the substrate in all three cases (See Fig 34). It should decrease the rate of emission coming from complex quasi-particles like trions and biexcitons since the density of charges is lower and also most of the photo-excited carriers will be transferred onto the substrate. However, it is not the case. If we look at the photoluminescence spectra at room temperature (Fig 33) we see that most of the contribution, in all cases, is coming from trions. So it can be understood in two ways, the first one is a high density of defects in the substrate like small holes or peaks, that change the strength on the monolayer, as well as defects in the transfer process that give place to cracks, folds, and wrinkles in the monolayer that enables the accumulation of charge. The second way is the short recombination rate the exciton that needs to emit in the WS_2 monolayer [94], which enables more efficient recombination before the charge to be transferred to the substrate.

Also, if we compare the PL of WS_2 with the one obtained for MoS_2 and WSe_2, it exhibits a stronger luminescence in all the substrates. This agrees with the second hypothesis. Trion lifetime should be short (suggested by its short value for excitons: 0.17 *ns* and 2.3 *ps* at room and low temperature respectively), compared with that for the MoS_2 and WSe_2 cases [94].

Analyzing our PL results in Figure 33 based on our proposed band alignment at room temperature (Figure 34), we can see that for the n-doped substrate, a few amounts of charges from the monolayer are transferred to the substrate, and could be said that the junction has a negative net charge. Thus, when light excites the junction, the photo-generated electrons in the single layer can be either transferred into the substrate or be bound to a defect in the junction. For those charges accumulated in the monolayer, an excess of electrons will occur owing to the net charge of the layer. This also will give rise to trion emerging and emission, in this case, negatively charged.

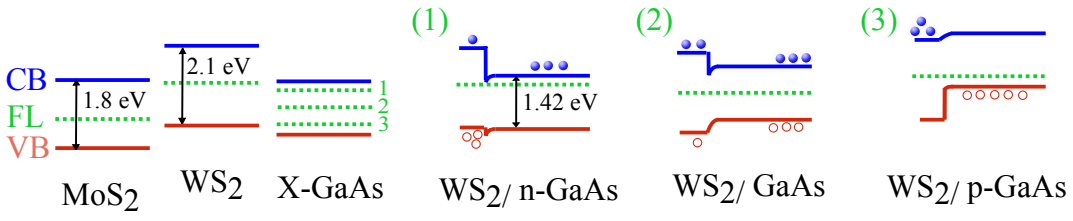

Figure 34 – Band alignment diagram proposed for WS_2/X-GaAs junctions.

In the case of the undoped substrate, we observe that excitons produced in the monolayer will have a high probability to be transferred to the substrate since the minimum of energy for holes and electrons is placed in it. Thus, even that trion emission can be

expected from the different kinds of defects, this junction should have a low charge concentration. The latter can be conferred on the Table 6 where the lower intensity ratio between trion and exciton emission is observed in the undoped case. Another possible reason is that this sample could have a bigger area without defects (See Fig 32), reducing the number of charges trapped in the monolayer.

	Room Temperature
Substrate	I_T/I_A
n-GaAs	4.35
GaAs	2.42
p-GaAs	3.12

Table 6 – Relative intensities of the emission peaks in the PL spectrum of WS_2 on different GaAs substrates.

For the sample on the p-doped substrate, a high static charge transfer to the substrate is produced. When electrons are photo-excited, they will find its energy minimum in the WS_2 single layer. However, after some time, most of the photo-generated holes will be transferred to the GaAs. Thus a low hole density in the valence band and a high electron density in the conduction band can enhance the negatively charged trion emission. From our proposed band offset in this case, it is expected a high exciton dissociation due to the large hole transference from the TMD to the substrate. However, as mentioned before, defects assist the TMD emission of excitons and trions, in this case negatively doped, owing to the excess of negative charge in the conduction band.

The low temperature measurements reveal a different shift for the spectral position of the emission for the p-doped GaAs sample in comparison with the n-GaAs and undoped cases. It is also worth noting that the shift in all cases is smaller than expected compared to the shift observed for MoS_2. From the literature, we can see that, at low temperatures, close to 11K, the reported emission peaks for exciton and trion are close to 592 nm (2.094 eV) and 600 nm (2.066 eV) [72]. Also in those works it is reported a high contribution of localized states. It means that the peaks we are looking to, are composed in good part from those states. The problem is that the spectral resolution provided by the spectrometer is not enough to resolve and identify approximate positions of each peak. This is why in Figure 33 the low-temperature spectra are presented without any peak adjustment. More detailed measurements, such as, for example, a detailed study of the evolution of the spectra as a function of the temperature, are needed to clarify these results.

Photoluminescence maps for the WSe_2 samples are shown in Figure 35. A high defect density is observed in the undoped and p-doped samples but also a high contrast to the substrate, suggesting a higher emission compared with the n-GaAs. This different behavior will be also observed in the photoluminescence spectra and the relative PL

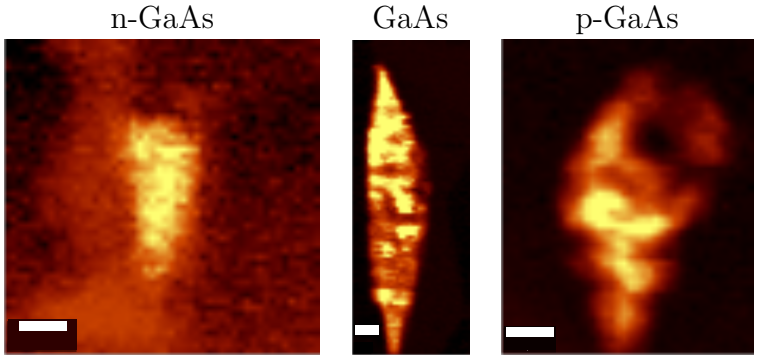

Figure 35 – WSe_2 PL maps of the red areas shown in the Figure 24. The scale bar is 3 μm in all panels; the PL maps do not have the same color scale.

intensities.

In Figure 36 we can see that at room temperature the spectra are dominated by A exciton emission with small contributions from trions. This behavior is also observed in other substrates like SiO_2 [52, 95]. From the relative intensities of the exciton and trion peaks, in Table 7, we observe that there are a higher amount of trions in the undoped substrate. Thus, there is a high density of charges in the monolayer in this junction. Looking to the band offset in Figure 37 most of the photoexcited electrons in the monolayer should be transferred to the substrate while the opposite situation is produced for holes in the valence band.

	Room Temperature	Low Temperature
Substrate	I_T/I_A	I_T/I_A
n-GaAs	0.23	10.32
GaAs	0.32	3.77
p-GaAs	0.19	2.75

Table 7 – Relative intensities of the emission peaks in the PL spectrum of WSe_2 on different GaAs substrates.

For the negatively doped substrate, this behavior is more accentuated, obtaining a high density of holes and a small one for electrons, in the single layer. This suggests that the trion identity of this junction should have a positively charged character. On the other hand, the positively doped substrate should have a high density of negative charges a small one of the positive ones. The latter suggests the presence of negative trions.

Low temperature measurements reveals two new peaks that were previously reported for WSe_2 deposited on Si/SiO_2 and which were associated to localized states [46] [96]. Particularly, *Huang et al.* [96] determine the identity of the exciton and trion peaks by studying the power and temperature dependence of each one. Defects in the lattice, as well as impurities produced during the fabrication process, can give origin to potential wells

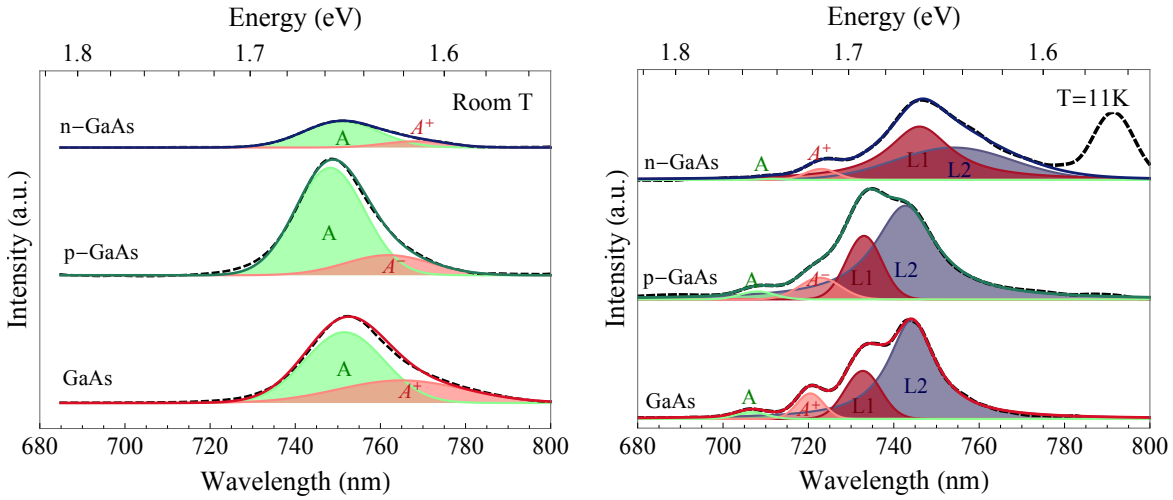

Figure 36 – PL spectra for the WSe_2 samples at room temperature (left) and T=11K (right). Experimental data (dashed lines) and fits (continuous line) are shown.

trapping the free excitons in the layer in a less energetic state. Due to the spontaneous character of these defects and the energy match of our spectra with the *Huang et al.* results, a GaAs substrate effect is less probable for those emissions.

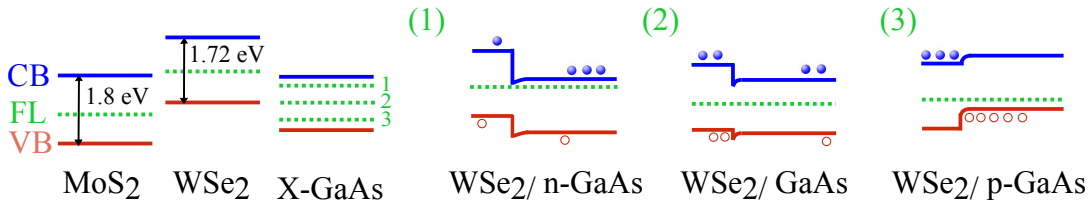

Figure 37 – Band alignment diagram proposed for WSe_2/X-GaAs junctions.

Nevertheless, we can still compare the relative intensities from the exciton and trion peaks. We can see (Table 7) a high difference in this ratio on the n-doped substrate, from room to low temperature as well as compared to any other substrate. To understand this change we should consider an important feature of layered materials: there is a gap between the monolayer and the substrate. The van der Waals character of the junction generates a gap that restricts the amount of charge that can be transferred among the materials. In addition to this, we should remember that the excitons in TMDs have a small radius and thus, they are highly localized into the layer.

When the temperature decreases, the distance among the two materials is reduced and thus, charge transfer is optimized [97]. This reduces the number of recombinations of excitons in the monolayer. Meanwhile, the trion emission is associated with defects that do not affect the distance in the interface of the materials, like cracks, vacancies or regions partially suspended.

It is worth noting that the sample in the n-doped substrate has a different behavior

not just in the intensity ratio, but also in the PL map as well as the lineshape of the PL at low temperature. In the latter, we can even see that photoluminescence coming from the substrate was so strong, and large, that the filter at $800nm$ was not able to eliminate all of its contributions and a remaining emission (dotted peak) is observed as well. The position and lineshape of the localized defects, in this case, is also different. It agrees with our previous proposal of different kind of defects involved in it.

CHAPTER 5

Conclusions and perspectives

We have studied Raman and PL spectra of the three main TMDs: MoS_2, WS_2 and WSe_2, over undoped, p and n-doped GaAs substrates. We developed a deterministic method of transference of the TMD monolayers on GaAs substrates despite the low optical contrast between the two materials. We studied the PL spectra at room and low temperature and propose band offset for the TMD-GaAs system for the three TMDs structures studied.

Many factors should be taken into account to describe the charge transfer in these systems. Some can come from the substrate, as impurities or physical defects; and others can come from the monolayer which, in the large majority, are produced during the transfer process, such as cracks, wrinkles, folds or even residual glue from the transfer tape. Some others can be produced during the time, like vacancies in the single-layer lattice, produced by oxidation and interaction with the laser. Features like the size of the van der Waals gap in monolayer/substrate interface, and the lifetime of the particles, also play an important role in the charge transfer process.

Despite that we were expecting a strong PL quenching based on the band alignment of the junctions, the reduction in the intensity was not so strong. We attribute this to different kinds of defects in the samples that reduce the number of charges transferred. In particular, the van der Waals gap in the interface can be one of the important features to take into account for the understanding of this process.

An analysis of the photoluminescence emission was made by studying the ratio of the trion and exciton peaks that allows us to infer the charge of the observed trion emission. Furthermore, an exciton dissociation is expected in most of the cases with the

exception of the MoS_2 and WS_2 samples in the undoped substrate in which a full exciton transfer will be more probable.

A high density of charge was observed, in particular, for the WS_2 samples. It was associated with smaller exciton and trion lifetimes, which makes the recombination process more efficient and reduces the PL quenching by the charge transfer process. On the other hand, low-temperature measurements allowed us to observe emission of localized states. In particular, for the sample in the n-doped substrate a different lineshape was observed. We attribute these emissions to defects that are not affected by the interface distance, such as cracks, folds, and vacancies.

For future work, we will make a deeper study on the defect features and characterization in the sample to reduce their density and improve the signal coming from the TMD monolayer and the substrate. Different substrate cleaning processes will be tested as well as other physical characterization methods such as atomic force microscopy (AFM) will be explored.

Also, we want to make measurements of the PL spectra evolution at different temperature values and, in this way, confirm the peak identity of all the PL spectra, with a particular interest in the WS_2 samples. Power dependence of the spectra can also give us information about the origin of the emissions and give a more solid support to our conclusions. Charge transfer between the materials could also be confirmed by making time-resolved PL measurements and studying the substrate luminescence after the single layer excitation to determine if an increase of the GaAs emission is produced **after** TMD excitation.

Finally, by configuring our experimental setup we want also to make low temperature PL maps, which will give us much more information about the spectral dependence of the monolayer position on the substrate.

Bibliography

[1] Lin, Shisheng, Xiaoqiang Li, Peng Wang, Zhijuan Xu, Shengjiao Zhang, Huikai Zhong, Zhiqian Wu, Wenli Xu, and Hongsheng Chen: *Interface designed MoS2/GaAs heterostructure solar cell with sandwich stacked hexagonal boron nitride.* Scientific reports, 5(May):15103, 2015, ISSN 2045-2322. `http://www.ncbi.nlm.nih.gov/pubmed/26458358{%}5Cnhttp://www.pubmedcentral.nih.gov/articlerender.fcgi?artid=PMC4602223`. Citado 3 vezes nas páginas 9, 28, and 48.

[2] Xu, Zhijuan, Shisheng Lin, Xiaoqiang Li, Shengjiao Zhang, Zhiqian Wu, Wenli Xu, Yanghua Lu, and Sen Xu: *Monolayer MoS2/GaAs heterostructure self-driven photodetector with extremely high detectivity.* Nano Energy, 23:89–96, 2016, ISSN 22112855. `http://dx.doi.org/10.1016/j.nanoen.2016.03.011`. Citado 3 vezes nas páginas 9, 12, and 29.

[3] Hao, Lanzhong, Yunjie Liu, Zhide Han, Zhijie Xu, and Jun Zhu: *Large Lateral Photovoltaic Effect in MoS2/GaAs Heterojunction.* Nanoscale Research Letters, 12(1):562, 2017, ISSN 1931-7573. `http://nanoscalereslett.springeropen.com/articles/10.1186/s11671-017-2334-z`. Citado 2 vezes nas páginas 9 and 30.

[4] Buscema, Michele, Gary A. Steele, Herre S J van der Zant, and Andres Castellanos-Gomez: *The effect of the substrate on the Raman and photoluminescence emission of single-layer MoS2.* Nano Research, 7(4):561–571, 2014, ISSN 19980124. Citado 4 vezes nas páginas 9, 22, 31, and 32.

[5] Novoselov, K. S., A. K. Geim, S V Morozov, D Jiang, Y Zhang, S V Dubonos, I V Grigorieva, A A Firsov, and K. S. Novoselov: *Electric Field Effect in Atomically Thin Carbon Films.* Science, 306:666–669, 2004, ISSN 0036-8075.

http://www.nature.com/doifinder/10.1038/nmat1849{%}0Ahttp://www.jstor.org/stable/3839379{%}5Cnhttp://about.jstor.org/terms. Citado na página 11.

[6] Elias, D. C., R. R. Nair, T. M. G. Mohiuddin, S. V. Morozov, P. Blake, M. P. Halsall, A. C. Ferrari, D. W. Boukhvalov, M. I. Katsnelson, and A. K. Geim: *Control of graphene's properties by reversible hydrogenation:evidence for graphene*. Science, (January):610–613, 2009. Citado na página 11.

[7] Mak, Kin Fai, Changgu Lee, James Hone, Jie Shan, and Tony F Heinz: *Atomically thin MoS2: A new direct-gap semiconductor*. Physical Review Letters, 105(13):2–5, 2010, ISSN 00319007. Citado 2 vezes nas páginas 12 and 19.

[8] Mak, Kin Fai and Jie Shan: *Photonics and optoelectronics of 2D semiconductor transition metal dichalcogenides*. Nature Publishing Group, 10, 2016. Citado na página 12.

[9] Splendiani, Andrea, Liang Sun, Yuanbo Zhang, Tianshu Li, Jonghwan Kim, Chi yung Chim, Giulia Galli, and Feng Wang: *Emerging Photoluminescence in Monolayer MoS 2*. Nano Letters, 10(4):1271–1275, apr 2010, ISSN 1530-6984. http://pubs.acs.org/doi/abs/10.1021/nl903868w. Citado 2 vezes nas páginas 12 and 20.

[10] Li, Hai, Zongyou Yin, Qiyuan He, Hong Li, Xiao Huang, Gang Lu, Derrick Wen Hui Fam, Alfred Iing Yoong Tok, Qing Zhang, and Hua Zhang: *Fabrication of single- and multilayer MoS 2 film-based field-effect transistors for sensing NO at room temperature*. Small, 8(1):63–67, 2012, ISSN 16136810. Citado na página 12.

[11] Lopez-Sanchez, Oriol, Dominik Lembke, Metin Kayci, Aleksandra Radenovic, and Andras Kis: *Ultrasensitive photodetectors based on monolayer MoS 2*. Nature Nanotechnology, 8(7):497–501, 2013, ISSN 17483395. Citado na página 12.

[12] *Hydrogen gas sensing properties of MoS2/Si heterojunction*. Sensors and Actuators, B: Chemical, 211:537–543, 2015, ISSN 09254005. Citado na página 12.

[13] Tsai, Meng Lin, Sheng Han Su, Jan Kai Chang, Dung Sheng Tsai, Chang Hsiao Chen, Chih I. Wu, Lain Jong Li, Lih Juann Chen, and Jr Hau He: *Monolayer MoS2 heterojunction solar cells*. ACS Nano, 8(8):8317–8322, 2014, ISSN 1936086X. Citado na página 12.

[14] Tonndorf, Philipp, Robert Schmidt, Robert Schneider, Johannes Kern, Michele Buscema, Gary A. Steele, Andres Castellanos-Gomez, Herre S. J. van der Zant, Steffen Michaelis de Vasconcellos, and Rudolf Bratschitsch: *Single-photon emission from localized excitons in an atomically thin semiconductor*. Optica,

2(4):347, 2015, ISSN 2334-2536. https://www.osapublishing.org/abstract.cfm?URI=optica-2-4-347. Citado na página 12.

[15] Castellanos-Gomez, Andres: *Why all the fuss about 2D semiconductors?* Nature Publishing Group, 10, 2016. Citado na página 12.

[16] Sun, Yinghui, Rongming Wang, and Kai Liu: *Substrate induced changes in atomically thin 2-dimensional semiconductors: Fundamentals, engineering, and applications.* Applied Physics Reviews, 4, 2017. http://dx.doi.org/10.1063/1.4974072http://aip.scitation.org/toc/are/4/1. Citado 2 vezes nas páginas 12 and 22.

[17] Drüppel, Matthias, Thorsten Deilmann, Peter Krüger, and Michael Rohlfing: *Diversity of trion states and substrate effects in the optical properties of an MoS2 monolayer.* Nature Communications, 8(1):2117, 2017, ISSN 2041-1723. http://www.nature.com/articles/s41467-017-02286-6. Citado na página 12.

[18] *Structural, optical and electrostatic properties of single and fewlayers MoS2: Effect of substrate.* 2D Materials, 2(1), 2015, ISSN 20531583. Citado na página 12.

[19] Mccreary, Kathleen M, Aubrey T Hanbicki, Simranjeet Singh, K Roland, and Berend T Jonker: *Substrate Sensitivity of Monolayer WS 2.* Sci. Rep., 6:35154, 2016. Citado na página 12.

[20] Cao, Bingchen, Xiaonan Shen, Jingzhi Shang, Chunxiao Cong, Weihuang Yang, Mustafa Eginligil, and Ting Yu: *Low temperature photoresponse of monolayer tungsten disulphide.* APL Materials, 2(11), 2014, ISSN 2166532X. Citado na página 13.

[21] Korn, T., S. Heydrich, M. Hirmer, J. Schmutzler, and C. Schller: *Low-temperature photocarrier dynamics in monolayer MoS2.* Applied Physics Letters, 99(10):2–5, 2011, ISSN 00036951. Citado na página 13.

[22] Christopher, Jason W., Bennett B. Goldberg, and Anna K. Swan: *Long tailed trions in monolayer MoS2: Temperature dependent asymmetry and resulting red-shift of trion photoluminescence spectra.* Scientific Reports, 7(1):1–8, 2017, ISSN 20452322. http://dx.doi.org/10.1038/s41598-017-14378-w. Citado 3 vezes nas páginas 13, 47, and 50.

[23] Park, Youngsin, Christopher C.S. Chan, Robert A. Taylor, Yongchul Kim, Nammee Kim, Yongcheol Jo, Seung W. Lee, Woochul Yang, Hyunsik Im, and Geunsik Lee: *Temperature induced crossing in the optical bandgap of mono and bilayer MoS2on SiO2.* Scientific Reports, 8(1):8–13, 2018, ISSN 20452322. Citado na página 13.

[24] Wilson, J. A. and A. D. Yoffe: *The transition metal dichalcogenides discussion and interpretation of the observed optical, electrical and structural properties.* Advances in Physics, 18(73):193–335, 1969, ISSN 14606976. Citado na página 14.

[25] Kertesz, Miklos and Roald Hoffmann: *Octahedral vs. Trigonal-Prismatic Coordination and Clustering in Transition-Metal Dichalcogenides*. (7):3453–3460, 1984. Citado na página 14.

[26] Kolobov, Alexander V. and Junji Tominaga: *Two-Dimensional Transition-Metal Dichalcogenides*, volume 239. Springer, 2016, ISBN 978-3-319-31449-5. `http://link.springer.com/10.1007/978-3-319-31450-1`. Citado 2 vezes nas páginas 14 and 18.

[27] Manzeli, Sajedeh, Dmitry Ovchinnikov, Diego Pasquier, Oleg V. Yazyev, and Andras Kis: *2D transition metal dichalcogenides*. Nature Reviews Materials, 2, 2017, ISSN 20588437. Citado na página 14.

[28] Jiménez Sandoval, S., D. Yang, R. Frindt, and J. Irwin: *Raman study and lattice dynamics of single molecular layers of MoS2*. Physical Review B, 44(8):3955–3962, 1991, ISSN 0163-1829. Citado na página 15.

[29] Lucovsky, G., R. M. White, J. A. Benda, and J. F. Revelli: *Infrared-reflectance spectra of layered group-IV and group-VI transition-metal dichalcogenides*. Physical Review B, 7(8):3859–3870, 1973, ISSN 01631829. Citado na página 15.

[30] Kohn, W: *Nobel Lecture: Electronic structure of matter—wave functions and density functionals*. Reviews of Modern Physics, 71(5):1253–1266, 1999, ISSN 0034-6861. `http://link.aps.org/doi/10.1103/RevModPhys.71.1253{\protect\T1\textdollar}{%}5C{\protect\T1\textdollar}nhttp://journals.aps.org/rmp/pdf/10.1103/RevModPhys.71.1253`. Citado na página 16.

[31] Kormányos, A., G. Burkard, M. Gmitra, J. Fabian, V. Zólyomi, N. D. Drummond, and V. Fal'ko: *$K \cdot P$ Theory for Two-Dimensional Transition Metal Dichalcogenide Semiconductors*. 2D Materials, 2(2):022001, 2015, ISSN 2053-1583. `http://stacks.iop.org/2053-1583/2/i=2/a=022001`. Citado na página 16.

[32] Ridolfi, E, D Le, T S Rahman, E R Mucciolo, and C H Lewenkopf: *A tight-binding model for MoS 2 monolayers*. Journal of Physics: Condensed Matter, 27:22, 2015. Citado na página 16.

[33] Liu, Gui Bin, Wen Yu Shan, Yugui Yao, Wang Yao, and Di Xiao: *Three-band tight-binding model for monolayers of group-VIB transition metal dichalcogenides*. Physical Review B - Condensed Matter and Materials Physics, 88(8):1–10, 2013, ISSN 10980121. Citado na página 16.

[34] Rostami, Habib, Ali G. Moghaddam, and Reza Asgari: *Effective lattice Hamiltonian for monolayer MoS2: Tailoring electronic structure with perpendicular electric and*

magnetic fields. Physical Review B - Condensed Matter and Materials Physics, 88(8):1–8, 2013, ISSN 10980121. Citado na página 16.

[35] Sun, Yajing, Dong Wang, and Zhigang Shuai: *Indirect-to-Direct Band Gap Crossover in Few-Layer Transition Metal Dichalcogenides: A Theoretical Prediction*. Journal of Physical Chemistry C, 120(38):21866–21870, 2016, ISSN 19327455. Citado 2 vezes nas páginas 16 and 18.

[36] Ashcroft, Neil and David Mermin: *Solid State Physics*. Number Autumn. Books/Cole, 1976, ISBN 0030839939. Citado 2 vezes nas páginas 17 and 25.

[37] Einstein, A: *The Quantum Theory of Radiation*. Physikalische Zeitschrift, 18:121, 1917, ISSN 0028-0836. `http://www.nature.com/articles/138483a0`. Citado na página 17.

[38] Xiao, Di, Gui Bin Liu, Wanxiang Feng, Xiaodong Xu, and Wang Yao: *Coupled spin and valley physics in monolayers of MoS 2 and other group-VI dichalcogenides*. Physical Review Letters, 108(19):1–5, 2012, ISSN 00319007. Citado 2 vezes nas páginas 17 and 19.

[39] Zhu, Z. Y., Y. C. Cheng, and U. Schwingenschl??gl: *Giant spin-orbit-induced spin splitting in two-dimensional transition-metal dichalcogenide semiconductors*. Physical Review B - Condensed Matter and Materials Physics, 84(15):1–5, 2011, ISSN 10980121. Citado na página 18.

[40] Wang, Haining, Changjian Zhang, and Farhan Rana: *Ultrafast dynamics of defect-assisted electron-hole recombination in monolayer MoS2*. Nano Letters, 15(1):339–345, 2015, ISSN 15306992. Citado na página 19.

[41] Liu, Hsiang Lin, Chih Chiang Shen, Sheng Han Su, Chang Lung Hsu, Ming Yang Li, and Lain Jong Li: *Optical properties of monolayer transition metal dichalcogenides probed by spectroscopic ellipsometry*. Applied Physics Letters, 105(20), 2014, ISSN 00036951. Citado 2 vezes nas páginas 19 and 21.

[42] Klots, A. R., A. K.M. Newaz, Bin Wang, D. Prasai, H. Krzyzanowska, Junhao Lin, D. Caudel, N. J. Ghimire, J. Yan, B. L. Ivanov, K. A. Velizhanin, A. Burger, D. G. Mandrus, N. H. Tolk, S. T. Pantelides, and K. I. Bolotin: *Probing excitonic states in suspended two-dimensional semiconductors by photocurrent spectroscopy*. Scientific Reports, 4:1–7, 2014, ISSN 20452322. Citado na página 19.

[43] He, Keliang, Nardeep Kumar, Liang Zhao, Zefang Wang, Kin Fai Mak, Hui Zhao, and Jie Shan: *Tightly bound excitons in monolayer WSe2*. Physical Review Letters, 113(2):1–5, 2014, ISSN 10797114. Citado na página 19.

[44] Plechinger, Gerd, Philipp Nagler, Ashish Arora, Andrés Granados del Águila, Mariana V. Ballottin, Tobias Frank, Philipp Steinleitner, Martin Gmitra, Jaroslav Fabian, Peter C. M. Christianen, Rudolf Bratschitsch, Christian Schüller, and Tobias Korn: *Excitonic valley effects in monolayer WS$_2$ under high magnetic fields*. 2016, ISSN 1530-6984. http://arxiv.org/abs/1612.03004{%}0Ahttp://dx.doi.org/10.1021/acs.nanolett.6b04171. Citado na página 19.

[45] Mak, Kin Fai, Keliang He, Changgu Lee, Gwan Hyoung Lee, James Hone, Tony F Heinz, and Jie Shan: *Tightly bound trions in monolayer MoS2*. Nature materials, 12(3):207–211, 2013, ISSN 1476-1122. http://dx.doi.org/10.1038/nmat3505. Citado 2 vezes nas páginas 19 and 20.

[46] Jones, Aaron M., Hongyi Yu, Nirmal J. Ghimire, Sanfeng Wu, Grant Aivazian, Jason S. Ross, Bo Zhao, Jiaqiang Yan, David G. Mandrus, Di Xiao, Wang Yao, and Xiaodong Xu: *Optical generation of excitonic valley coherence in monolayer WSe 2*. Nature Nanotechnology, 8(9):634–638, 2013, ISSN 17483395. Citado 2 vezes nas páginas 19 and 54.

[47] Wei, Ke, Yu Liu, Hang Yang, Xiangai Cheng, and Tian Jiang: *Large range modification of exciton species in monolayer WS_2*. Applied Optics, 55(23):6251, 2016, ISSN 0003-6935. https://www.osapublishing.org/abstract.cfm?URI=ao-55-23-6251. Citado na página 19.

[48] Mai, Cong, Andrew Barrette, Yifei Yu, Yuriy G. Semenov, Ki Wook Kim, Linyou Cao, and Kenan Gundogdu: *Many-body effects in valleytronics: Direct measurement of valley lifetimes in single-layer MoS2*. Nano Letters, 14(1):202–206, 2014, ISSN 15306984. Citado 2 vezes nas páginas 19 and 20.

[49] You, Yumeng, Xiao Xiao Zhang, Timothy C. Berkelbach, Mark S. Hybertsen, David R. Reichman, and Tony F. Heinz: *Observation of biexcitons in monolayer WSe 2*. Nature Physics, 11(6):477–481, 2015, ISSN 17452481. Citado 2 vezes nas páginas 19 and 20.

[50] Plechinger, Gerd, Philipp Nagler, Julia Kraus, Nicola Paradiso, Christoph Strunk, Christian Sch??ller, and Tobias Korn: *Identification of excitons, trions and biexcitons in single-layer WS2*. Physica Status Solidi - Rapid Research Letters, 9(8):457–461, 2015, ISSN 18626270. Citado na página 19.

[51] Fox, Mark: *Optical Properties of Solids*. Oxford University Press, New York, NY, 2001. Citado 2 vezes nas páginas 20 and 22.

[52] Van 't Erve, Olaf M.J., Aubrey T. Hanbicki, Adam L. Friedman, Kathleen M. McCreary, Enrique Cobas, Connie H. Li, Jeremy T. Robinson, and Berend T. Jonker:

Graphene and monolayer transition-metal dichalcogenides: Properties and devices. Journal of Materials Research, 31(7):845–877, 2016, ISSN 20445326. Citado 3 vezes nas páginas 21, 37, and 54.

[53] Li, Yuanyuan, Zeming Qi, Miao Liu, Yuyin Wang, Xuerui Cheng, Guobin Zhang, and Liusi Sheng: *Photoluminescence of monolayer MoS2 on LaAlO3 and SrTi3 substrates.* Nanoscale, 6(24):15248–15254, 2014, ISSN 2040-3364. `http://xlink.rsc.org/?DOI=C4NR04602A`. Citado 2 vezes nas páginas 22 and 23.

[54] Sercombe, D, S Schwarz, O Del Pozo-Zamudio, F Liu, B J Robinson, E a Chekhovich, I I Tartakovskii, O Kolosov, and a I Tartakovskii: *Optical investigation of the natural electron doping in thin MoS2 films deposited on dielectric substrates.* Scientific reports, 3:3489, 2013, ISSN 2045-2322. `http://www.pubmedcentral.nih.gov/articlerender.fcgi?artid=3860010{&}tool=pmcentrez{&}rendertype=abstract`. Citado na página 22.

[55] Scheuschner, Nils, Oliver Ochedowski, Anne Marie Kaulitz, Roland Gillen, Marika Schleberger, and Janina Maultzsch: *Photoluminescence of freestanding single- and few-layer MoS 2.* Physical Review B - Condensed Matter and Materials Physics, 89(12):2–7, 2014, ISSN 1550235X. Citado 2 vezes nas páginas 23 and 24.

[56] Yu, Yifei, Yiling Yu, Chao Xu, Yong Qing Cai, Liqin Su, Yong Zhang, Yong Wei Zhang, Kenan Gundogdu, and Linyou Cao: *Engineering Substrate Interactions for High Luminescence Efficiency of Transition-Metal Dichalcogenide Monolayers.* Advanced Functional Materials, 26(26):4733–4739, 2016, ISSN 16163028. Citado na página 23.

[57] Zhou, S. Y., G. H. Gweon, A. V. Fedorov, P. N. First, W. A. De Heer, D. H. Lee, F. Guinea, A. H. Castro Neto, and A. Lanzara: *Substrate-induced bandgap opening in epitaxial graphene.* Nature Materials, 6(10):770–775, 2007, ISSN 14764660. Citado na página 23.

[58] Chang, Hsiao Yu, Shixuan Yang, Jongho Lee, Li Tao, Wan Sik Hwang, Debdeep Jena, Nanshu Lu, and Deji Akinwande: *High-performance, highly bendable MoS2 transistors with high-K dielectrics for flexible low-power systems.* ACS Nano, 7(6):5446–5452, 2013, ISSN 19360851. Citado na página 23.

[59] Pu, Jiang, Yohei Yomogida, Keng Ku Liu, Lain Jong Li, Yoshihiro Iwasa, and Taishi Takenobu: *Highly flexible MoS 2 thin-film transistors with ion gel dielectrics.* Nano Letters, 12(8):4013–4017, 2012, ISSN 15306984. Citado na página 23.

[60] Kay, Nicholas D, Benjamin J Robinson, Vladimir I Fal, Konstantin S Novoselov, and Oleg V Kolosov: *Electromechanical Sensing of Substrate Charge Hidden under Atomic 2D Crystals.* 2014. Citado na página 23.

[61] Liu, Kai, Qimin Yan, Michelle Chen, Wen Fan, Yinghui Sun, Joonki Suh, Deyi Fu, Sangwook Lee, Jian Zhou, Sefaattin Tongay, Jie Ji, B Neaton, and Junqiao Wu: *Elastic Properties of Chemical-Vapor-Deposited Monolayer MoS 2 , WS 2 , and Their Bilayer Heterostructures.* 2014. Citado 2 vezes nas páginas 23 and 24.

[62] Conley, Hiram J, Bin Wang, Jed I Ziegler, Richard F Haglund, Sokrates T Pantelides, and Kirill I Bolotin: *Bandgap Engineering of Strained Monolayer and Bilayer MoS 2.* pages 1–5, 2013. Citado na página 24.

[63] Man, Michael K.L., Skylar Deckoff-Jones, Andrew Winchester, Guangsha Shi, Gautam Gupta, Aditya D. Mohite, Swastik Kar, Emmanouil Kioupakis, Saikat Talapatra, and Keshav M. Dani: *Protecting the properties of monolayer MoS2 on silicon based substrates with an atomically thin buffer.* Scientific Reports, 6(January):1–9, 2016, ISSN 20452322. `http://dx.doi.org/10.1038/srep20890`. Citado na página 24.

[64] Hjort, M., S. Lehmann, J. Knutsson, R. Timm, D. Jacobsson, E. Lundgren, K. A. Dick, and A. Mikkelsen: *Direct imaging of atomic scale structure and electronic properties of GaAs wurtzite and zinc blende nanowire surfaces.* Nano Letters, 13(9):4492–4498, 2013, ISSN 15306984. Citado na página 25.

[65] Srnánek, R., A. Vincze, D. McPhail, S. Littlewood, A. Kromka, and E. Jánoš: *Optical properties of GaAs based layers characterised by Raman spectroscopy and photoluminescence.* ASDAM 2000 - Conference Proceedings: 3rd International EuroConference on Advanced Semiconductor Devices and Microsystems, pages 307–310, 2000. Citado na página 25.

[66] Wan, Kam and Jeff F. Young: *Interaction of longitudinal-optic phonons with free holes as evidenced in Raman spectra from Be-doped p-type GaAs.* Physical Review B, 41(15):10772–10779, 1990, ISSN 01631829. Citado na página 25.

[67] Nathan, M. I., W. P. Dumke, K. Wrenner, S. Tiwari, S. L. Wright, and K. A. Jenkins: *Electron mobility in p-type GaAs.* Applied Physics Letters, 52(8):654–656, 1988, ISSN 00036951. Citado na página 25.

[68] Blakemore, J. S.: *Semiconducting and other major properties of gallium arsenide.* Journal of Applied Physics, 53(10), 1982, ISSN 00218979. Citado na página 25.

[69] Yu, Peter and Manuel Cardona: *Fundamentals of Semiconductors.* Springer, fourth edition, 2010, ISBN 9783642007095. Citado na página 25.

[70] Irmer, G, J Monecke, and S Griehl: *Micro Raman Study of Dislocations in n-Type Doped GaAs 0.* Journal of Raman Spectroscopy, 24(June):761–766, 1993. Citado na página 25.

[71] Yi, Min and Zhigang Shen: *A review on mechanical exfoliation for the scalable production of graphene.* Journal of Materials Chemistry A, 3(22):11700–11715, 2015, ISSN 20507496. Citado na página 26.

[72] Yao, Huizhen, Lai Liu, Zhuo Wang, Henan Li, Longlong Chen, Mei Er Pam, Weigang Chen, Hui Ying Yang, Yumeng Shi, and Wenjing Zhang: *Significant Photoluminescence Enhancement in WS2 Monolayers through Na2S Treatment.* Nanoscale, pages 6105–6112, 2018, ISSN 2040-3364. http://pubs.rsc.org/en/Content/ArticleLanding/2018/NR/C8NR00530C. Citado 2 vezes nas páginas 27 and 53.

[73] Samassekou, Hassana, Asma Alkabsh, Eaton Miller, Milinda Wasala, Andrew Walker, S. Talapatra, T Jayasekera, and D Mazumdar: *Viable route towards large-area two dimensional MoS 2 using magnetron sputtering.* 2D Materials, 4(2):21002, 2017, ISSN 2053-1583. http://stacks.iop.org/2053-1583/4/i=2/a=021002. Citado na página 27.

[74] Bosi, Matteo: *Growth and synthesis of mono and few-layers transition metal dichalcogenides by vapour techniques: A review.* RSC Advances, 5(92):75500–75518, 2015, ISSN 20462069. Citado na página 27.

[75] Li, Hai, Gang Lu, Zongyou Yin, Qiyuan He, Hong Li, Qing Zhang, and Hua Zhang: *Optical identification of single- and few-layer MoS2 Sheets.* Small, 8(5):682–686, 2012, ISSN 16136810. Citado na página 30.

[76] Castellanos-Gomez, Andres, Michele Buscema, Rianda Molenaar, Vibhor Singh, Laurens Janssen, Herre S J van der Zant, and Gary A Steele: *Deterministic transfer of two-dimensional materials by all-dry viscoelastic stamping.* 2D Materials, 1(1):011002, 2014, ISSN 2053-1583. http://stacks.iop.org/2053-1583/1/i=1/a=011002?key=crossref.4a11185bed3e80db2f125d0422bf4c4b. Citado na página 33.

[77] *Refractive index database.* https://refractiveindex.info/. Accessed: 2018-07-16. Citado na página 35.

[78] Aspnes, D. E., S. M. Kelso, R. A. Logan, and R. Bhat: *Optical properties of AlxGa1-xAs.* Journal of Applied Physics, 60(2):754–767, 1986, ISSN 00218979. Citado na página 35.

[79] Zhang, Hui, Yaoguang Ma, Yi Wan, Xin Rong, Ziang Xie, Wei Wang, and Lun Dai: *Measuring the refractive index of highly crystalline monolayer MoS2 with high confidence.* Scientific reports, 5:8440, 2015, ISSN 2045-2322. http://www.nature.com/srep/2015/150213/srep08440/full/srep08440.html{%}7B{#}{%}7Dsupplementary-information. Citado na página 35.

[80] Aspnes, D. E. and A. A. Studna: *Dielectric functions and optical parameters of Si, Ge, GaP, GaAs, GaSb, InP, InAs, and InSb from 1.5 to 6.0 eV*. Physical Review B, 27(2):985–1009, 1983, ISSN 01631829. Citado na página 35.

[81] Tonndorf, Philipp, Robert Schmidt, Philipp Böttger, Xiao Zhang, Janna Börner, Andreas Liebig, Manfred Albrecht, Christian Kloc, Ovidiu Gordan, Dietrich R T Zahn, Steffen Michaelis de Vasconcellos, and Rudolf Bratschitsch: *Photoluminescence emission and Raman response of monolayer MoS_2, MoSe_2, and WSe_2*. Optics Express, 21(4):4908, 2013, ISSN 1094-4087. `https://www.osapublishing.org/oe/abstract.cfm?uri=oe-21-4-4908`. Citado 2 vezes nas páginas 36 and 45.

[82] *WITec focus innovations*. `https://www.witec.de/`. Accessed: 2018-07-26. Citado na página 37.

[83] Li, Hong, Qing Zhang, Chin Chong Ray Yap, Beng Kang Tay, Teo Hang Tong Edwin, Aurelien Olivier, and Dominique Baillargeat: *From bulk to monolayer MoS 2: Evolution of Raman scattering*. Advanced Functional Materials, 22(7):1385–1390, 2012, ISSN 1616301X. Citado 2 vezes nas páginas 41 and 44.

[84] Li, Xiao and Hongwei Zhu: *Two-dimensional MoS2: Properties, preparation, and applications*. Journal of Materiomics, 1(1):33–44, 2015, ISSN 23528478. `http://linkinghub.elsevier.com/retrieve/pii/S2352847815000040`. Citado na página 41.

[85] Berkdemir, Ayse, Humberto R. Gutiérrez, Andrés R. Botello-Méndez, Néstor Perea-López, Ana Laura Elías, Chen Ing Chia, Bei Wang, Vincent H. Crespi, Florentino López-Urías, Jean Christophe Charlier, Humberto Terrones, and Mauricio Terrones: *Identification of individual and few layers of WS2 using Raman Spectroscopy*. Scientific Reports, 3(1):1755, 2013, ISSN 2045-2322. `http://www.nature.com/articles/srep01755`. Citado 3 vezes nas páginas 42, 44, and 45.

[86] Terrones, H., E. Del Corro, S. Feng, J. M. Poumirol, D. Rhodes, D. Smirnov, N. R. Pradhan, Z. Lin, M. A.T. Nguyen, A. L. Elías, T. E. Mallouk, L. Balicas, M. A. Pimenta, and M. Terrones: *New First Order Raman-active Modes in Few Layered Transition Metal Dichalcogenides*. Scientific Reports, 4:1–9, 2014, ISSN 20452322. Citado na página 45.

[87] Li, H., X. Zhu, Z. K. Tang, and X. H. Zhang: *Low-temperature photoluminescence emission of monolayer MoS2 on diverse substrates grown by CVD*. Journal of Luminescence, 199(March):210–215, 2018, ISSN 00222313. Citado na página 47.

[88] Varshni, Y.P.: *Temperature dependence of the energy gap in semiconductors*. Physica, 34(1):149–154, 1967, ISSN 00318914. `http://linkinghub.elsevier.com/retrieve/pii/0031891467900626`. Citado na página 47.

[89] McCreary, Kathleen M., Aubrey T. Hanbicki, Saujan V. Sivaram, and Berend T. Jonker: *A- and B-exciton photoluminescence intensity ratio as a measure of sample quality for transition metal dichalcogenide monolayers*. APL Materials, 6(11), 2018, ISSN 2166532X. http://dx.doi.org/10.1063/1.5053699. Citado na página 49.

[90] Kang, Jun, Sefaattin Tongay, Jian Zhou, Jingbo Li, and Junqiao Wu: *Band offsets and heterostructures of two-dimensional semiconductors*. Applied Physics Letters, 102(1), 2013, ISSN 00036951. Citado na página 52.

[91] Xiao, Jingwei, Yu Zhang, Huanjun Chen, Ningsheng Xu, and Shaozhi Deng: *Enhanced Performance of a Monolayer MoS2/WSe2 Heterojunction as a Photoelectrochemical Cathode*. Nano-Micro Letters, 10(4):60, 2018, ISSN 2311-6706. http://link.springer.com/10.1007/s40820-018-0212-6. Citado na página 52.

[92] Li, Chao, Xiao Yan, Xiongfei Song, Wenzhong Bao, and Shijin Ding: *WSe2/MoS2 and MoTe2/SnSe2 van der Waals heterostructure transistors with different band alignment*. 2017. Citado na página 52.

[93] Hill, Heather M., Albert F. Rigosi, Kwang Taeg Rim, George W. Flynn, and Tony F. Heinz: *Band Alignment in MoS ₂ /WS ₂ Transition Metal Dichalcogenide Heterostructures Probed by Scanning Tunneling Microscopy and Spectroscopy*. Nano Letters, 16(8):4831–4837, 2016, ISSN 1530-6984. http://pubs.acs.org/doi/10.1021/acs.nanolett.6b01007. Citado na página 52.

[94] Palummo, Maurizia, Marco Bernardi, and Jeffrey C. Grossman: *Exciton radiative lifetimes in two-dimensional transition metal dichalcogenides*. Nano Letters, 15(5):2794–2800, 2015, ISSN 15306992. Citado na página 52.

[95] Yan, Tengfei, Xiaofen Qiao, Xiaona Liu, Pingheng Tan, and Xinhui Zhang: *Photoluminescence properties and exciton dynamics in monolayer WSe ₂*. Applied Physics Letters, 105(10):101901, 2014, ISSN 0003-6951. http://aip.scitation.org/doi/10.1063/1.4895471. Citado na página 54.

[96] Huang, Jiani, Thang B. Hoang, and Maiken H. Mikkelsen: *Probing the origin of excitonic states in monolayer WSe2*. Scientific Reports, 6(August 2015):1–7, 2016, ISSN 20452322. http://dx.doi.org/10.1038/srep22414. Citado na página 54.

[97] Zhang, Linglong, Han Yan, Xueqian Sun, Miheng Dong, Tanju Yildirim, Bowen Wang, Bo Wen, Guru Prakash Neupane, Ankur Sharma, Yi Zhu, Jian Zhang, Kun Liang, Boqing Liu, Hieu T. Nguyen, Daniel Macdonald, and Yuerui Lu: *Modulated interlayer charge transfer dynamics in a monolayer TMD/metal junction*. Nanoscale, 11(2):418–425, 2019, ISSN 2040-3364. http://xlink.rsc.org/?DOI=C8NR08728H. Citado na página 55.

Appendix

APPENDIX A

Data filtering

Due to the high PL intensity of the substrate, most of the samples should be filtered by subtracting the substrate PL from the monolayer PL to observe the light coming just from the TMD . Then, a low-pass filter is used to clean the signal for the subsequent fitting to produce the spectra presented in chapter 4. Figure 38 presents an example of the filtration process which we followed for the data analysis.

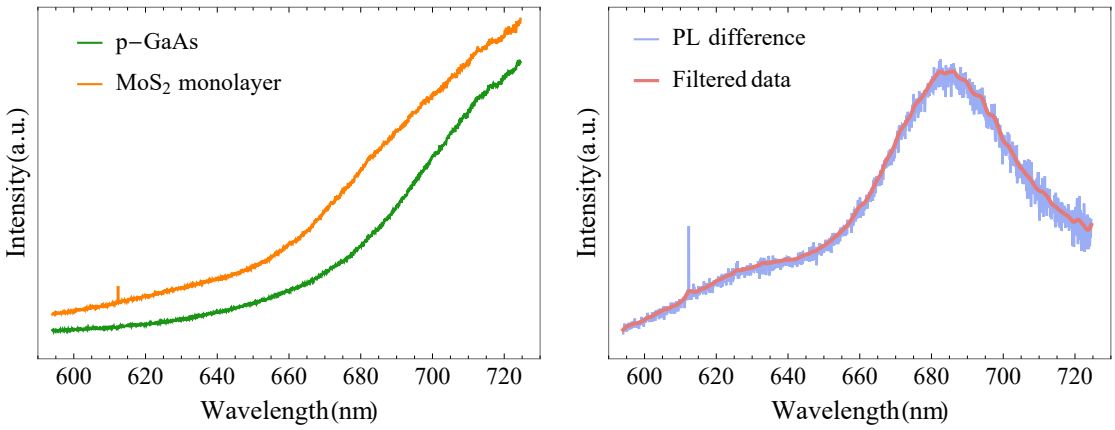

Figure 38 – Room temperature PL spectra for the MoS_2 single layer on p-GaAs substrate. Raw data (left), the PL difference and its filtering (right).

APPENDIX B

PL experimental values

MoS_2						
Substrate	Room T			Low T		
	B	A	A^*	B	A	A^*
n-GaAs	638	678	–	585	655	686
p-GaAs	632	684	–	–	645	668
GaAs	633	683	704	587	642	665

Table 8 – Experimental values of the PL peaks, in nm, of the MoS_2 monolayers.

WS_2						
Substrate	Room T			Low T		
	B	A	A^*	B	A	A^*
n-GaAs	–	625	637	–	–	623
p-GaAs	–	624	637	–	–	616
GaAs	–	624	637	–	–	627

Table 9 – Experimental values of the PL peaks, in nm, of the WS_2 monolayers.

WSe_2						
Substrate	Room T		Low T			
	A	A^*	A	A^*	L_1	L_2
n-GaAs	751	768	710	723	746	754
p-GaAs	748	761	708	722	733	742
GaAs	751	765	706	720	732	744

Table 10 – Experimental values of the PL peaks, in nm, of the WSe_2 monolayers.